Self-management of ROV umbilical using sliding element: A general 3D-model

Christophe Viel

Self-Management of ROV Umbilical using sliding element: a general 3D-model

Christophe Viel*

* CNRS, Lab-STICC, F-29806, Brest, France (e-mail: name.surname@ensta-bretagne.fr).

ARTICLE INFO

Keywords:
Underwater robotics, cables management, cables model

ABSTRACT

The umbilical of Remote Operated Vehicle (ROV) has two main problems: it is subject to entanglement with obstacles or itself, and its shape is difficult to predict for navigation. To address these issues, this article proposes a passive self-management of an ROV's umbilical by adding one or two elements, like ballasts, buoys, or an oriented thruster, to stretch it and gives it a predictable shape. These elements can be fixed or move freely on the umbilical. In opposite with [36, 37], we propose a general model which can estimate the shape of the umbilical in three-dimensions regardless of the orientation of the force applied to the elements, allowing to consider the presence of underwater currents, passive or motorized elements on the tether, and the presence or absence of TMS. Several examples of umbilical configurations are proposed, each one adapted for ROV exploration in various environments, including near-surface, seafloor, near-wall, and dive between obstacles. The model is compared with results proposed in other works like [36, 37]. The limits of the method are discussed.

Part I
Introduction, state-of-art, contribution

1. Introduction

Underwater umbilicals serve to connect an underwater Remotely Operated Vehicle (ROV) to a control unit or Human-Machine Interface typically situated on a boat. This umbilical, or tether, serves three primary functions: enable real-time bidirectional data transmission, supplying energy to the ROV, and preventing the loss of the robot during exploration [27]. Real-time bidirectional transmission enables operators to receive video feedback, control inputs, and instrument measurements instantaneously (see [6, 33]). The energy delivered by the cable makes the ROV particularly advantageous for maintenance operations and underwater worksites compared to autonomous underwater vehicles (AUVs): AUVs' battery capacities are insufficient for prolonged usage of large tools, necessitating the use of ROVs for energy-intensive tasks. ROVs find applications in offshore exploration [42], monitoring fishing reserves [40], underwater archaeology [23], pipeline inspection [32], marine growth removal [30], and more. The umbilical is also used for Remotely Operated Towed Vehicle (ROTV), where its importance surpasses that for ROVs because it provides its propulsion underwater [13, 29]. The tether provides to the ROTVs distinct advantages over both ROVs and AUVs for large area exploration, research and data collection: as they are not self-propelled like ROVs and AUVs, ROTV can cover a larger area faster [21]. However, umbilicals have drawbacks such as collision risks, impact on ROV maneuverability due to umbilical inertia and drag forces, entanglement, and cable breakage. In the case of ROTV, the controller must carefully take into account the shape of the umbilical to safely maneuver the ROTV away from obstacles and prevent damage. Designing the umbilical involves balancing the constraints of the umbilical, battery power, and real-time feedback for optimal ROV performance [7].

Understanding the shape of the umbilical holds two main advantages. Firstly, designing the umbilical's parameters before diving helps avoid weight-related issues and reduces the risk of entanglement by using a cable that is appropriately sized. Secondly, real-time knowledge of the umbilical shape during the dive enables operators to prevent self-entanglement or collisions with known obstacles in a mapped environment or detected by sensors such as sonar or vision systems. In the literature, umbilicals have been modelled and instrumented to provide feedback on their position and shape. Two main categories of methods exist: detection/feedback of the umbilical shape using for example vision [25, 24, 26] and/or sensors placed directly on or in the umbilical [16, 10], or direct modelling of the umbilical using boat and ROV positions [18, 17, 19, 12, 37, 5], sometimes accounting for sea current information. While the first category offers accurate real-time shape estimation, it often requires expensive umbilical equipment and complex sensor setups, making modeling methods more appealing for cost-effective obstacle avoidance. In opposite, this second category of methods have the advantage of being implementable for all kinds of umbilicals, but are often less accurate and cannot always provide results in real-time.

Various methods are available for modeling the cable's shape and dynamics. These range from simple geometrical models like the catenary curve [34, 8, 9] to segment-based models with geometrical constraints [18, 17]. Geometrical models can simulate a large number of segments in real-time and are memory-efficient when precise physical modeling is

ORCID(s):

not necessary. For cases requiring accurate cable dynamics, the Lumped-mass-spring method [4, 19, 20] and the segmental method are commonly used [11, 12, 2, 5]. The former represents the umbilical as mass points interconnected by massless elastic elements, while the latter treats the cable as a continuous system and solves the resulting partial differential equations numerically.

The umbilical can also be equipped. A Tether Management System (TMS) [1] is a subsea winch controlled by a human operator and attached to the ROV cage. The TMS helps regulate the length of the tether cable to maintain the umbilical taut. However, this system adds weight to the cable and can be operationally complex. Some research explores automation or alternative solutions, such as using an Unmanned Surface Vehicle (USV) [35, 22], a secondary ROV [26], multiple ROVs, or a motorized plug/float assembly [3]. In [9, 8], an estimation of the catenary tether shape connecting a pair of underwater robots is performed using data acquired from inertial measurement units (IMUs) attached to the cable near its ends. To provide a fast time computational model of the cable, the main author [37, 36] has proposed to equip the umbilical with ballasts or buoys moving freely on the cable, allowing it to be stretched and given a predictable shape. The umbilical can therefore be assimilated to predictable straight lines, simple to model and compute calculate in real time. Nonetheless, these systems still rely on knowledge of various ROV parameters, such as its position.

This paper proposes proposes a passive self-management of an ROV's umbilical by adding one or two elements, like ballasts, buoys or an oriented thruster, to stretch it and gives it a predictable shape. These elements can be fixed or move freely on the umbilical, restrained to a specific part of the cable with stops to prevent the elements from staying constantly in contact. In opposite with our previous work [36, 37], a general model is proposed which can estimate the shape of the umbilical in three-dimension regardless of the orientation of the force applied to the elements. This model allows also to consider presence of underwater currents, passive or motorized elements on the tether, and presence or not of TMS.

The main contributions are

- a self-management of the umbilical to stretch it and so avoid self-entanglement. This one can be passive using only sliding ballasts and buoys using only weight and Archimedes force, or active using motorized thruster or TMS;
- a method simple to add to existing ROVs with a light and simple setup;
- a general model of the umbilical in three-dimensions which can consider the presence of underwater currents or external forces, helping the operator to prevent collisions with environmental obstacles.

The umbilical is modeled using geometrical relations and the Fundamental Principle of Static (FPS). Depending on the umbilical configurations, the resolution will be performed analytically or numerically. Numerical performance are discussed

The paper is divided in five parts. Part I introduces the problem in Section 1 and the related work in Section 2.

Part II groups the umbilical model, the assumptions taken, definitions and properties of the umbilical and elements studied. The problematic and assumptions considered are described in Section 3. The geometrical model of the umbilical is presented in Section 4. The dynamics of the system are studied in Section 4.2.

To solve the geometric and dynamics model, different configurations of the umbilical can be observed depending of the position of the moving elements on the cable. These different configurations and their particularities are described in Part III.

Part IV presents theorems allowing to solve the system in function of the current configuration of the umbilical.

Part V discusses of the numerical resolution of the problem, proposes possible umbilical configuration/equipment adapted for specific missions, discuss of the limits of the model based on simulation and experimentation. Section 11 concludes the work.

2. Related work

2.1. Cable modeling

Various methods are available for modeling the shape and dynamics of cables. The simplest model is the catenary curve [34], which describes a non-neutral, non-rigid flexible cable in water. However, for longer or heavier cables, additional parameters such as bending stiffness need to be considered. In other methods like [18, 17], neutrally buoyant cables are assumed, allowing the gravity and buoyancy forces to be ignored. These methods involve modeling the umbilical as a chain of segments with geometric constraints to account for its stiffness. While these geometric models may not be physically accurate or consider cable dynamics, they offer fast calculations and are memory efficient.

In [37, 36] the umbilical is equipped with ballasts or buoys moving freely on the cable giving it a predictable shape. The umbilical can therefore be assimilated to predictable straight lines, simple to model and compute calculate in real time. Dynamic effects are approximated by the assumption of quasi-static equilibrium. The method however stills rely on knowledge of parameters like ROV's position and forces applied on the sliding elements, and considers only a 2 dimensional case without horizontal underwater current. Moreover, the model cannot also handle cables longer than 50 meters or complex dynamics movements.

For a dynamic and physically accurate cable model, two main types of methods exist as discussed in [2]: the lumped-mass-spring method[4, 19, 20] and the segmental method [11, 12]. The lumped-mass-spring method represents the

umbilical as mass points connected by massless elastic elements. On the other hand, the segmental method treats the cable as a continuous system and numerically solves the resulting partial differential equations. These two methods primarily focus on cable dynamics in simplified environments, considering forces such as gravity, buoyancy, hydrodynamic drag, environmental inertial force, axial tension, twisting force, and bending force. However, they generally require substantial computing resources. In [12], a three-dimensional ROV-cable model is presented, utilizing the Euler-Bernoulli beam theory modified to allow for cable compression. Building on the beam equation, [5] derives a realistic 3D model of tether dynamics and approximates it via the Finite Element Method (FEM), which can be executed in real time. The method is however only tested in simulation. [13] studies a fossen model of a ROTV and an umbilical cable modeled by a lumped mass-spring approach, validated against real test data. Results shows that by accounting for the uncertainties of hydrodynamic parameters and unknown underwater environment disturbances, these simple models can estimate the real ROTV steady-state operation which can be simulated close to real-time. The study is however performed for short umbilical (4 meters), with computation time linearly increasing with the number of nodes.

Cable modeling is also study for fishing gear, complex mechanical structures mainly composed of netting and cables. The aim is to design efficient, eco-friendly gear with enhanced catch and reduced environmental impact. [19] presents several cable models for real-time simulation of maneuvers with submerged cables and fishing gear. Using linear-spring and multibody cable models comprised to a few thousand variables, real-time simulations of let-out and reel-in manoeuvres with submerged cables can be obtained. Simulations with other rigid body elements and assemblies like doors, anchors, and selective devices are possibles. A parallel implementations is necessary to obtain a fast computation.

2.2. Cable instrumentation

The umbilical can be equipped and instrumented to provide feedback on its position and shape. In the literature, two main categories of methods are discussed: vision-based detection of the umbilical [25, 24, 26], and the use of sensors embedded directly in the umbilical [16, 10]. These methods offer accurate real-time modeling but require specific, expensive, and complex equipment.

In [16], the "Smart Tether" method is introduced, which uses IMU sensor nodes embedded in the umbilical to provide real-time information about its shape and motion. However, this method is costly and introduces irregularities along the cable, making winding problematic. In [10], optic fibers are braided within the umbilical and use interferometry properties to monitor the cable's 3D curve in real time. Again, this solution is expensive (around 200,000 euros for 50m length).

For shallow-water exploration, [9, 8, 26] proposes an estimation of the shape of a catenary for a negatively buoyant cable, connecting a pair of underwater robots. First estimated using camera-based detection and tracking of a constant distance between the ROVs in [26, 25, 24], the method is then in [9, 8] based on the calculation of local tangents thanks to the data acquired from inertial measurement units (IMUs), attached to the cable near its ends. Unlike [25], the identification of the cable shape is not affected by the limits of the camera's field of view and image projection. Combining it with the study in [37], an improvement is proposed in [38] by equipping the umbilical with moving ballasts and buoys to give it a predictable shape with straight lines, in opposite with the catenary curve trickier to estimate.

Additional components such as TMS, ballasts, buoys, or intermediate cables can be used as dampers to mitigate undesired forces on the ROV caused by waves, underwater currents, or the weight of the umbilical. For deep and ultra-deep-water operations, [28] proposes alternative configurations to minimize umbilical tension and the risk of snapping, such as installing a series of floaters along the umbilical. However, floaters increase the ROV's offset and sensitivity to currents. The TMS is a common equipment choice, acting as an underwater winch attached to the ROV's cage to regulate the tether length and maintain tension. Indeed, tether length has an impact on the ROV navigation due to the inertia and drag forces applied on it. In [31], a dynamics model is developed to simulate the dynamics of variable length tether and investigate a dynamic positioning system for a tethered underwater vehicle. The cable is equipped with floats to relieve some of the cable's weight. Coupled with a winch PD controller to vary the umbilical length, it offers a significant reduction in the tether induced disturbance force on the vehicle. However, TMS is not suitable for umbilicals equipped with a large number of buoys or ballasts that interfere with the cable winding. Note that when placed underwater, TMS can also serves as a ballast to reduce ROV offset due to underwater currents and waves.

Due to the complexity of TMS operation, efforts have been made to automate or replace it with other vehicles such as USVs or secondary ROVs [26, 3, 35]. In [3], a motorized plug/float assembly moves along the umbilical to adjust its buoyancy, even allowing it to temporarily behave like an AUV. The cable length is regulated by a winch on the boat. While this system offers flexibility, it is large, expensive, and not suitable for all ROV applications. In [35, 22], an integrated system consisting of a USV with an embedded winch, an umbilical, and an ROV is proposed to provide various cable management options. The distance between the USV and the ROV can be adjusted to control the tension in the umbilical and avoid collisions with underwater obstacles. A segmental method-based mechanical behavior model is proposed in the study. In [37, 36], the addition of ballast and a buoy or two buoys moving freely on the umbilical prevents self-entanglement of the cable by stretching it without motorization, and gives it a predictable shape. Different shape of umbilical obtained with ballasts

and buoys, allowing to explore close to the surface, seafloor exploration, or dive easily in a cluttered environment.

2.3. Umbilical impact on ROV mission

Depending on the size of the ROV and its mission, the tether can have different impacts and constraints. If the tether serves as a power supply or lifeline, its size is typically proportional to the ROV's dimensions. Larger ROVs often necessitate thicker tethers to meet higher power requirements or support their weight during ascent without risking breakage. For ROTVs, the cable must withstand the force exerted by water and currents when pulled by the boat. These cables are often wide, rigid, and heavy. On the other hand, if the tether is primarily used for communication, a smaller one may suffice. Smaller ROVs can benefit from lighter and more flexible tethers, enhancing maneuverability during exploration.

The density of the cable also affects ROV control. Neutral cables or those with minimal buoyancy/weight impose less strain on the ROV, but they are prone to tangling. Poorly managed cables can also become entangled with cables from other ROVs when they work in close proximity. Floating/diving cables facilitate exploration at seabed/sea surface, as they naturally move away from areas with obstacles, but they create tension at the rear of the ROV, requiring it to be strong enough to counteract this force. Similarly, the longer the cable, the greater the risk of it being caught up in marine currents, thereby adding extra constraints to the ROV. TMS are employed to minimize the cable's length to the necessary minimum, mitigating its exposure to currents. These systems can be positioned either upstream of the cable or behind the ROV. When positioned behind the ROV, the cable is usually laid on the seabed to prevent it from being carried away by the current (e.g., for karstic exploration). Nonetheless, managing the cable length for deployment or retraction isn't always simple, so leaving a surplus of cable provides flexibility for the ROV.

Part II
Umbilical model, assumption, properties

3. Problematic and assumption

3.1. Notation

Consider the indirect referential $\mathcal{R}$ where the vertical axis is oriented to the ground such that $y = 0$ corresponds to the sea level and $y_1 > y_2$ means that y_1 is deeper than y_2. The umbilical is attached between $O = (0,0,0)$ and $R = (x,y,z)$, the boat's and ROV's coordinates. Let define $\vec{e}_x = \begin{bmatrix} 1 & 0 & 0 \end{bmatrix}^T$, $\vec{e}_y = \begin{bmatrix} 0 & 1 & 0 \end{bmatrix}^T$ and $\vec{e}_z = \begin{bmatrix} 0 & 0 & 1 \end{bmatrix}^T$. Let $\vec{a}.\vec{b}$ be the scalar product of two vector $\vec{a} \in \mathbb{R}^3$ and $\vec{b} \in \mathbb{R}^3$. For the two arguments (x,y), the function atan2 is defined as $\phi = \text{atan2}(y,x) = \text{Arg}(x+iy)$ with $-\pi < \text{atan2}(y,x) \leq \pi$.

For a variable a, let note $a_{\mathcal{R}_b}$ the variable in a referential $\mathcal{R}_b$. In order to lighten notations, the notations $v_{\mathcal{R}_b} = \begin{bmatrix} a_{\mathcal{R}_b} & b_{\mathcal{R}_b} & c_{\mathcal{R}_b} \end{bmatrix}^T$ and $v_{\mathcal{R}_b} = \begin{bmatrix} a & b & c \end{bmatrix}^T_{\mathcal{R}_b}$ are equivalent. By default and unless otherwise specified in the current section, parameters are expressed in $\mathcal{R}$ ($x_{\mathcal{R}}$ is noted x). Let note $M_x(\theta)$, $M_y(\theta)$ and $M_z(\theta)$ the rotation matrices of angle θ respectively around axis $\vec{x}$, $\vec{y}$ and $\vec{z}$.

For two lists $L_1 = \{a,b\}$ and $L_2 = \{c,d\}$, $L_1 \cup L_2 = \{a,b,c,d\}$ is the union of the lists and $L_3 = \{L_1, L_2\} = \{\{a,b\},\{c,d\}\}$ is a list of lists.

3.2. Problematic

In the absence of tension, a cable can move freely and take an irregular shape. To prevent it from becoming entangled with itself or its environment, a common technique for shallow dives is to suspend a ballast at a fixed length on the umbilical, stretching the portion between the boat and the ballast. However, the part between the ballast and the ROV remains loose, especially when the ROV is close to the boat, where it takes the shape of a bell. In order to keep the umbilical taut independently of the robot position, we propose to equip the umbilical with other elements to stretch it and give it a geometrical shape that is simple to model and predict. In opposite with [36, 37], the model proposed here considers three-dimensional case and a general orientation of the forces applied on the umbilical.

Additional elements attached to the cable (ex: ballast, buoy) can be defined as "fixed" or "sliding". A fixed element can usually only stretch one part of it, both in particular configuration. A sliding element however finds its position at its minimum potential energy where it stretches both parts of the cable simultaneously (corresponding to the lowest/highest position possible in case of ballast/buoy). Sliding elements can be obtained using for example pulley, as illustrated in Figure 1 and used in [36, 37].

In this study, the Definition 1 defines the term "element" such that it takes into account both horizontal and vertical forces, making it possible to take into account the presence of underwater currents in addition to the forces exerted by the ballast/buoy, or to propose a motorized element pushing in a customized direction.

Definition 1. *An element i on the umbilical is defined by a vector $\vec{F}_i$ expressed as*

$$\vec{F}_i = \begin{bmatrix} \cos(\phi_i)\cos(\psi_{Fi}) \\ \sin(\phi_i)\cos(\psi_{Fi}) \\ \sin(\psi_{Fi}) \end{bmatrix} F_i \tag{1}$$

where F_i is the norm of the force applied on the cable, ψ_{Fi} is the orientation in the plan $O\vec{x}\vec{y}$ and $\phi_i \in \left[-\frac{\pi}{2}, \frac{\pi}{2}\right]$ is the angle of elevation from the plan $O\vec{x}\vec{y}$. Let's also define the notation $\vec{F}_i = \begin{bmatrix} F_{ix} & F_{iy} & F_{iz} \end{bmatrix}^T$.

An element is considered

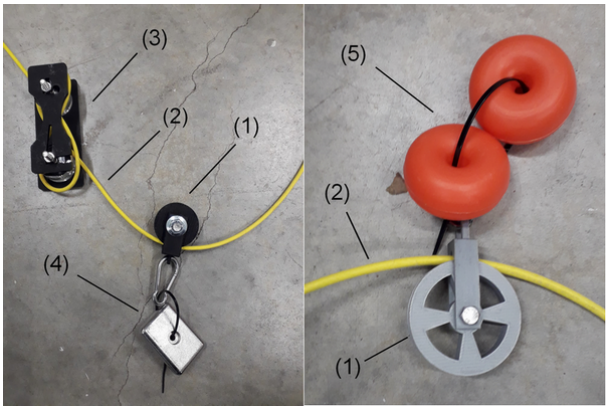

Figure 1: Examples of sliding siding elements made using pulley. 1: pulley, 2: umbilical, 3: stop element on the umbilical, 4: ballast to create a vertical downward force, 5: buoys to create a vertical ascending force.

- *"Sliding" if its point of application changes with the cable orientation. The movements of the sliding element are limited to a defined portion of the cable of length l_i. Let l_{i1} and l_{i2} be the two parts of the cable l_i on each side of the element i such $l_i = l_{i1} + l_{i2}$ with $l_i \geq l_{ij} \geq 0$ for $j \in \{1, 2\}$.*
- *"Fixed" if its point of application is constant on the cable. In this case, consider the element is at the end of its portion of cable, i.e. ones has $l_{i1} = l_i$ and $l_{i2} = 0$.*

A combination of sliding elements or fixed and sliding elements is an interesting solution to stretch the tether. To prevent the elements from remaining in contact in the same position (minimum potential energy), each sliding element must be contained on a specific part of the cable by stops. The umbilical is so divided into several parts with defined lengths. In the optic to make this study the most general possible, we consider here that the length of these parts can be modified using TMS at the end of the tether or at the stop position. Let's assume, however, that the length of these parts is always known.

In this paper, the umbilical is equipped with one or two elements at most, plus a possible anchor directly after the boat. Cases with more elements are not treated here because the solution will be too complex and/or inefficient. This point will be discussed in Section 10.3.

3.3. Assumption

Consider the umbilical is equipped with maximum two elements, plus a possible anchor directly after the boat (not necessarily on the seafloor). The following assumption are considered:

A1) The forces applied on the umbilical due to its mass and buoyancy are negligible compare to the action made by the elements and the anchor.

A2) The umbilical length is such that it is reasonable to neglect its length variation, considered as constant.

A3) When the umbilical is taut, its geometry can be assimilated to straight lines between defined points, here the elements, the boat and the ROV.

A4) Consider the ROV, boat and anchor are strong enough to compensate action of the cables and the elements, and therefore remain stationary. (x, y, z) is so fixed when ROV is not moving.

A5) Consider the sliding elements move freely on the umbilical without friction.

A6) The end of a cable connected to an anchor or to the boat is assumed to be perfectly fixed. A cable connected at both ends by the boat and the anchor does not need to meet the Assumption A1–A3.

A7) The lengths l_i of the different parts of the umbilical are supposed to be constant or known in real time. Possible TMS positioned on the boat, anchor or the ROV can be placed to effect these lengths.

A8) The influence of underwater currents and external perturbations are considered in the elements i.

In order to ensure assumptions A1 and A2, the application scope of the present system is for ROVs with an umbilical shorter than 50 m. In addition, to respect assumption A3, the current system requires that the umbilical is flexible and allows the sliding element to move freely along it. Therefore, the current method is suitable for the following scenarios:

- Exploration of shallow water from a boat with a depth of less than 50m, with zero or stable underwater currents.
- Ship's hull inspection, navigation under uniform ice, or other missions requiring a a flowing cable, flexible but not heavy.
- Umbilical between an ROV and its cage in case of deep exploration. The umbilical length is then measured from the cage, which is is considered as an anchor in this study. The cable between the boat and the cage, then, does not need to meet the assumptions described above, as described in Assumption A6.
- Chain of ROVs connected with the same umbilical, the model being applicable for each section of cable linking two consecutive ROVs.

Validity of the assumptions in these conditions have been observed in experiments, see Section 10.2.1. Some studies like [15] compare cables of varying stiffness, weight, and buoyancy to help determine which cables are compatible with a fair estimation of the cable shape. We can see that flexibility depends not only on the material used for the sheath but also on the components it contains and their number. During our experiments, a plastic umbilical with a two-pair network cable with a diameter of 4mm was used to obtain very good flexibility. The same model with a four-pair network cable and a diameter of 10 mm was stiffer

and required a heavier ballast to achieve the same results (involving other disadvantages).

Note that the shape of the umbilical cannot be assimilated to straight lines 1) when an element reaches the surface/seabed, 2) in some configurations when fixed elements are involved.

4. Description umbilical model

4.1. Geometrical model

The description made below consider a cable with two sliding elements and an anchor, named the general combination. Other combinations will be deduced from it.

The parameters are illustrated in Figure 2 in 2D, with an illustration of a 3D case in Figure 3. The umbilical of length l is divided in three parts. Let $l_0 = \|OA\| \geq 0$ be the part between the boat O and the anchor A, $l_1 = \|AS\| \geq 0$ the part between the anchor A and a stop S, and $l_2 = \|SR\| \geq 0$ the part between the stop S and the ROV R. The total length of the boat is $l = L + l_0$ with $L = l_1 + l_2$. The sliding elements B_1 and B_2 can respectively move freely on l_1 and l_2.

Following Assumption A6, the part l_0 is supposed to stay perfectly vertical. The sliding elements B_1 and B_2 create angles in the geometry of the umbilical. Note that the stop S does not create an angle by itself, so $\|B_1B_2\|$ is a straight line.

All the other combinations with fixed elements or a single element can be deduced from the general combination. Indeed:

- a fixed element i can be assimilated to a particular case of a sliding element i where $l_{i2} = 0$ (see Definition 1);
- the absence of anchor correspond to $l_0 = 0$;
- a combination with an unique element can be obtained taking $l_2 = 0$ and $F_2 = 0$.

The orientation of $\|AB_1\|$ is described by the oriented angle α_1 and ψ_1 such that

$$\begin{aligned}\overrightarrow{AB_1} = l_{11} &\left(\cos\left(\alpha_1\right)\cos\left(\psi_1\right)\vec{e}_x\right. \\ &\left.+\sin\left(\alpha_1\right)\cos\left(\psi_1\right)\vec{e}_y+\sin\left(\psi_1\right)\vec{e}_z\right)\end{aligned} \tag{2}$$

In the same way, one can define the orientation of $\|B_1B_2\|$ and $\|B_2R\|$ with angles (α_2, ψ_2) and (α_3, ψ_3) such that

$$\begin{aligned}\overrightarrow{B_1B_2} = \left(l_{12}+l_{21}\right) &\left(\cos\left(\alpha_2\right)\cos\left(\psi_2\right)\vec{e}_x\right. \\ &\left.+\sin\left(\alpha_2\right)\cos\left(\psi_2\right)\vec{e}_y+\sin\left(\psi_2\right)\vec{e}_z\right)\end{aligned} \tag{3}$$

$$\begin{aligned}\overrightarrow{B_2R} = l_{22} &\left(\cos\left(\alpha_3\right)\cos\left(\psi_3\right)\vec{e}_x\right. \\ &\left.+\sin\left(\alpha_3\right)\cos\left(\psi_3\right)\vec{e}_y+\sin\left(\psi_3\right)\vec{e}_z\right).\end{aligned} \tag{4}$$

Note that $\alpha_1 \in [-\pi, \pi]$, $\alpha_2 \in [-\pi, \pi]$, $\alpha_3 \in [-\pi, \pi]$ and $\psi_1 \in \left[-\frac{\pi}{2}, \frac{\pi}{2}\right]$, $\psi_2 \in \left[-\frac{\pi}{2}, \frac{\pi}{2}\right]$, $\psi_3 \in \left[-\frac{\pi}{2}, \frac{\pi}{2}\right]$. The vectors $\overrightarrow{B_1S}$ and $\overrightarrow{SB_2}$ can also be expressed

$$\begin{aligned}\overrightarrow{B_1S} = l_{12} &\left(\cos\left(\alpha_2\right)\cos\left(\psi_2\right)\vec{e}_x\right. \\ &\left.+\sin\left(\alpha_2\right)\cos\left(\psi_2\right)\vec{e}_y+\sin\left(\psi_2\right)\vec{e}_z\right)\end{aligned} \tag{5}$$

$$\begin{aligned}\overrightarrow{SB_2} = l_{21} &\left(\cos\left(\alpha_2\right)\cos\left(\psi_2\right)\vec{e}_x\right. \\ &\left.+\sin\left(\alpha_2\right)\cos\left(\psi_2\right)\vec{e}_y+\sin\left(\psi_2\right)\vec{e}_z\right).\end{aligned} \tag{6}$$

In a configuration where the umbilical is taut, the system can be expressed such

$$\begin{cases} x = & l_{11}\cos\left(\alpha_1\right)\cos\left(\psi_1\right)+\left(l_{12}+l_{21}\right)\cos\left(\alpha_2\right)\cos\left(\psi_2\right) \\ & +l_{22}\cos\left(\alpha_3\right)\cos\left(\psi_3\right) \\ y = & l_{11}\sin\left(\alpha_1\right)\cos\left(\psi_1\right)+\left(l_{12}+l_{21}\right)\sin\left(\alpha_2\right)\cos\left(\psi_2\right) \\ & +l_{22}\sin\left(\alpha_3\right)\cos\left(\psi_3\right)+l_0 \\ z = & l_{11}\sin\left(\psi_1\right)+\left(l_{12}+l_{21}\right)\sin\left(\psi_2\right)+l_{22}\sin\left(\psi_3\right) \end{cases} \tag{7}$$

Remark 1. *When $\alpha_1 = \alpha_2$ and $\psi_1 = \psi_2$, the portion of cable l_1 is perfectly straight. Same remark for l_2 when $\alpha_2 = \alpha_3$ and $\psi_2 = \psi_3$.*

Let's define $C_{A,r}$ the sphere of center $A = \begin{bmatrix} 0 & l_0 & 0 \end{bmatrix}$ and radius $r = l_1 + l_2$. Let's also define $\bar{C}_{A,r}$ the truncated sphere such as for all $(x, y, z) \in \bar{C}_{A,r}$, one has $(x, y, z) \in C_{A,r}$ and $y \geq 0$, *i.e.* $\bar{C}_{A,r} = \left\{(x, y, z) \in C_{A,r} | y \in [0, r]\right\}$. $\bar{C}_{A,r}$ corresponds to the underwater sphere where the ROV can move.

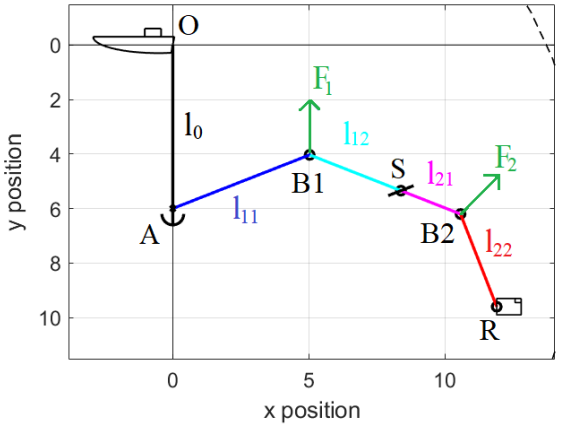

Figure 2: Parameters of the umbilical with two sliding elements B_1 and B_2 and an anchor A, in 2 dimension. $\vec{F}_1$ and $\vec{F}_2$ are the forces applied on the elements B_1 and B_2. Here $\vec{F}_1$ is a pure vertical force made for example by a buoy, and $\vec{F}_2$ is a combination of a vertical and horizontal forces, for example a buoy plus horizontal underwater currents.

Depending on the ROV's position, the sliding elements move and can come in contact 1) with the anchor A or the stop S for the element 1, 2) with the stop S or the ROV R for the element 2. To simplify the notations, let note S_i and S_{i+1} the stops that surround the element i such that the element i is in contact with S_i when $l_{i1} = 0$ and in contact with the S_{i+1} when $l_{i2} = 0$.Thus, one has $S_1 = A$ and $S_2 = S$ for the element 1, and $S_2 = S$ and $S_3 = R$ for the element 2.

The different cases representing when elements do or do not touch a stop are called "configurations" or "areas".

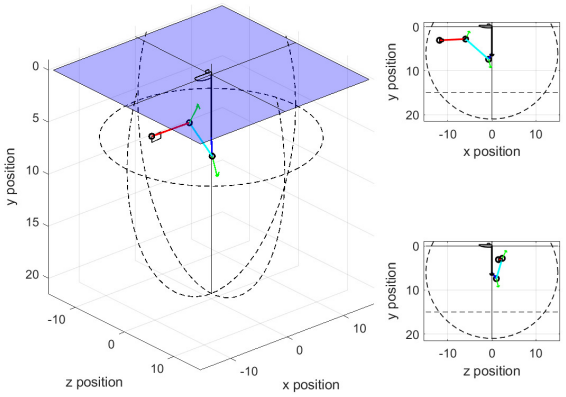

Figure 3: Illustration of the umbilical with two sliding elements and an anchor, in 3-Dimension.. $\vec{F}_1 = \begin{bmatrix} 0.5 & 2 & 0.5 \end{bmatrix}$ and $\vec{F}_2 = \begin{bmatrix} 0.5 & -1 & 0.5 \end{bmatrix}$.

The system is considered to be inside an area if the ROV coordinates (x, y, z) are inside this area. The different areas will be described in Section 5

4.2. Dynamic of the system

The systems presented in the following sections are studied in equilibrium. It should be noted that each time the ROV moves, part of the umbilical temporarily becomes loosen, which can lead to entanglement and invalidate the proposed model. As a loose cable is complex to model and/or computationally heavy, we propose to maintain a quasi-static equilibrium by controlling the ROV to shorten transient phases, thus minimizing the gap between proposed models and reality. In this way, the ROV is controlled to move more slowly than the elements on the cable: as long as their behavior is faster than the ROV speed, the umbilical will remain taut overall. Details of this approach are described in [37]. The same solution can be applied to manage the waves, see Section 10.5.

4.2.1. Fundamental Principle of Static

The dynamics of the system is studied at its equilibrium. Consider in this section than neither of the two elements touches the surface, the seafloor or an obstacle. Since there is not friction (Assumption A5), the Fundamental Principle of Static (FPS) on B_i can be expressed as

$$\vec{F}_i + \vec{T}_i + \vec{T}_{i+1} = 0 \tag{8}$$

where $\vec{T}_i$ and $\vec{T}_{i+1}$ are the tension of the umbilical applied on element i. Let's note $T_i = \left\|\vec{T}_i\right\| > 0$ and $\left\|\vec{T}_{i+1}\right\| = T_{i+1} > 0$.

Again, depending on the ROV's position, the sliding elements can come in contact with stop, changing the expression of the FPS. For an element $i \in \{1, 2\}$, if $B_1 \neq B_2$ and 1) $B_1 \neq A$ if $i = 1$ or 2) $B_2 \neq R$ if $i = 2$, one can perform the following FPS in B_i:

$$\begin{cases} -\cos(\psi_i)\cos(\alpha_i)\,T_i + \cos(\psi_{i+1})\cos(\alpha_{i+1})\,T_{i+1} \\ \quad +F_i\cos(\psi_{Fi})\cos(\phi_i) & = 0 \\ -\cos(\psi_i)\sin(\alpha_i)\,T_i + \cos(\psi_{i+1})\sin(\alpha_{i+1})\,T_{i+1} \\ \quad +F_i\cos(\psi_{Fi})\sin(\phi_i) & = 0 \\ -\sin(\psi_i)\,T_{1i} + \sin(\psi_{i+1})\,T_{i+1} + F_i\sin(\psi_{Fi}) & = 0 \end{cases} \tag{9}$$

with $T_i > 0$, $T_{i+1} > 0$, $F_i > 0$. (9) is also valid if element i is fixed.

In particular case where both elements are in contact, *i.e.* $B_1 = B_2$, one gets a single FPS in B_1:

$$\begin{cases} -\cos(\psi_1)\cos(\alpha_1)\,T_1 + \cos(\psi_3)\cos(\alpha_3)\,T_3 \\ \quad +F_{\Sigma x} & = 0 \\ -\cos(\psi_1)\sin(\alpha_1)\,T_1 + \cos(\psi_3)\sin(\alpha_3)\,T_3 \\ \quad +F_{\Sigma y} & = 0 \\ -\sin(\psi_1)\,T_1 + \sin(\psi_3)\,T_3 + F_{\Sigma z} & = 0 \end{cases} \tag{10}$$

where $\vec{F}_\Sigma = \vec{F}_1 + \vec{F}_2$ can be expressed as

$$\begin{bmatrix} F_{\Sigma x} \\ F_{\Sigma y} \\ F_{\Sigma z} \end{bmatrix} = \sum_{i=1}^{2} \left(\begin{bmatrix} \cos(\phi_i)\cos(\psi_{Fi}) \\ \sin(\phi_i)\cos(\psi_{Fi}) \\ \sin(\psi_{Fi}) \end{bmatrix} F_i \right) \tag{11}$$

From Assumption A4, the ROV, boat and anchor are strong enough to compensate action of the elements. Thus, when a element is in contact with the anchor A, boat O or the ROV R, element's action can be fuse with them and so no FPS are performed.

4.2.2. Sliding elements properties

Since the sliding element move freely on the tether, the tensions of the cable try to balance on both sides of the element. Thus, some properties can be defined, as described in Definition 2, Theorem 1 and illustrated in Figure 4.

Definition 2. *For the sliding element i, the following properties can be expressed:*

(1) If $\left(\vec{F}_i.\vec{T}_i < 0\right)$ & $\left(\vec{F}_i.\vec{T}_{i+1} < 0\right)$ *and* $\left(l_i > l_{i1} > 0\right)$ & $\left(l_i > l_{i2} > 0\right)$*, the sliding element i can move freely and is not in contact with a stop. Since the element slides without friction (Assumption A5), one has the property*

$$T_i = T_{i+1}. \tag{12}$$

(2) If $l_{i1} = 0$ *and* $\left(\vec{F}_i.\vec{T}_{i+1} < 0\right)$*, the element i is in stable contact with* S_i*. In this configuration, it can be assimilate to a fixed element. Reciprocally for* S_{i+1} *if* $l_{i2} = 0$ *and* $\left(\vec{F}_i.\vec{T}_i < 0\right)$.

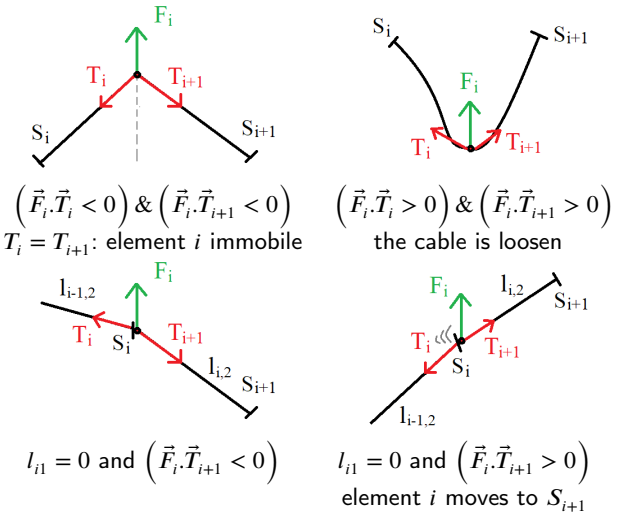

Figure 4: Illustration of the forces applied on the umbilical with a sliding element. The different cases correspond to the cases exposed in Definition 2.

(3) If $\vec{F}_i.\vec{T}_i > 0$, then the element i slides in the direction $\overrightarrow{B_iS_i}$ and so cannot stay in contact with S_{i+1}. Reciprocally in direction direction $\overrightarrow{B_iS_{i+1}}$ if $\vec{F}_i.\vec{T}_{i+1} > 0$.

(4) If $\left(\vec{F}_i.\vec{T}_i > 0\right) \& \left(\vec{F}_i.\vec{T}_{i+1} > 0\right)$, the cable is loosen.

Theorem 1. *For $i \in \{1, 2\}$, if the sliding element i is not in contact with a stop, then*

$$\cos\left(\psi_i\right)\sin\left(\phi_i - \alpha_i\right) = \cos\left(\psi_{i+1}\right)\sin\left(\phi_i - \alpha_{i+1}\right). \quad (13)$$

The proof of Theorem 1 can be found in [39, Appendix A]

Remark 2. *The condition $\left(\vec{F}_i.\vec{T}_i < 0\right)$ in Definition 2 can be replaced by the condition $\left(\vec{F}_i.\overrightarrow{B_iS_i} < 0\right)$.*

Same for $\left(\vec{F}_i.\vec{T}_{i+1} < 0\right)$ with $\left(\vec{F}_i.\overrightarrow{B_iS_{i+1}} < 0\right)$.

These properties will be used the next sections to solve the system (7) and estimate if a solution found is physically possible.

Part III
Resolution of the model: the problem of the configuration areas

5. Configuration areas of the umbilical

As already explained, depending on the ROV's position, the sliding elements can come in contact stops S, modifying the shape of the umbilical and the balance of the forces exerted on it. The different cases where elements do or do not touch a stop are called "configurations" or "areas". Each configuration therefore has its own geometrical particularity and dynamic model based on PFS due to the sliding elements properties described in Section 4.2.

The system is considered to be in a configuration if the ROV coordinates (x, y, z) are inside its associate area. In the 2D-case developed in [36, 37], it was possible to calculate the boundaries of these areas and thus deduce in which configuration the umbilical was in based of the ROV coordinate. In this way, the system was solved only once in its current area.

Unfortunately, it is not possible to find an expression of the boundaries areas in the 3D case in presence of horizontal forces, which makes the problem trickier to solve because we cannot known in which configuration the umbilical is and therefore how to express the geometric and dynamic systems. The system must so be solved in all configurations and results obtained must be compared to find the real solution, as it will be described in Section 6.4.

This section describes the different zones and their specific dynamics.

5.1. Description of the areas

Eight areas corresponding to specific umbilical configurations can be observed, plus the forbidden area F, as illustrate in Figures 5 and 6.

The different areas are described below:

- Area A0: the two elements move freely on l_1 and l_2, *i.e.* $0 < l_{11} < l_1$, $0 < l_{12} < l_1$, $0 < l_{21} < l_2$, $0 < l_{22} < l_2$.
- Area A1: the element 1 moves freely on l_1, *i.e.* $0 < l_{11} < l_1$, $0 < l_{12} < l_1$. Moreover:
  - Area A11: the element 2 is in contact with R, thus $l_{21} = l_2$, $l_{22} = 0$.
  - Area A12: the element 2 is in contact with S, thus $l_{21} = 0$, $l_{22} = l_2$.
- Area A2: the element 2 moves freely on l_2, *i.e.* $0 < l_{21} < l_2$, $0 < l_{22} < l_2$. Moreover:
  - Area A21: the element 1 is in contact with A, thus $l_{11} = 0$, $l_{12} = l_1$.
  - Area A22: the element 1 is in contact with S, thus $l_{11} = l_1$, $l_{12} = 0$.
- Area D: both elements are in contact with a stop such that
  - Area D1: the element 1 is in contact with S and element 2 is in contact with R, $l_{11} = l_1$, $l_{12} = 0$, $l_{21} = l_2$, $l_{22} = 0$.
  - Area D2: the two elements are in contact with S, *i.e.* $l_{11} = l_1$, $l_{12} = 0$, $l_{21} = 0$, $l_{22} = l_2$.
  - Area D3: the element 1 is in contact with A and element 2 is in contact with S, *i.e.* $l_{11} = 0$, $l_{12} = l_1$, $l_{21} = 0$, $l_{22} = l_2$.

case	Element 1	Element 2	Existing areas	Remark
1	sliding	sliding	A0*, A11, A12, A21, A22, D1, D2, D3, F	A0*: depend of the direction of the element force
2	fixed	sliding	A22, D1, D2, F	$l_{11} = l_1$. Else, see case 5
3	sliding	fixed	A12, D2, D3, F	$l_{21} = 0$. Else, see case 5
4	fixed	fixed	D3, F	equivalent to one element in S. $l_{11} = l_1$ and $l_{21} = 0$
5	sliding	/	A11, D1, D3, F	One element configuration.
6	fixed	/	F	the cable cannot be taut excepted as a straight line

Table 1
Existing areas in function of the number and type of element. Note that a fixed element is always fixed in S. Else, it is assimilate to the anchor A or the ROV R (Assumption A4).

- Area F. The forbidden area F includes 1) the inaccessible area for the ROV due to the length of its umbilical, 2) the areas where the umbilical cannot be taut by the elements, 3) case where an element is in contact with the seabed/surface.

In function of the number and characteristic of the elements on the umbilical, some configurations cannot exist. Area A0 for example cannot exist in presence of two forces in the same direction (example: two buoys) because one of the element will always be in contact with a stop, see Theorem 2. When the element 1 is fixed, Areas 21 and Areas 22 does not exist.

The Table 1 summarizes the existing area in function of the configurations.

Definition 3. *When the cable l_1 is perfectly straight, i.e. $\alpha_1 = \alpha_2$ and $\psi_1 = \psi_2$, the sliding element 1 has no obstacle on this path. Since we consider there is no friction (Assumption A5) and to remove any ambiguity, we also assume that the sliding element can only be in contact with a stop, even in the case where $\vec{F}_1$ and $\overrightarrow{AB_1}$ are perpendicular. Same remark for element 2 if l_2 is straight. In this condition:*

(1) The configuration $(\alpha_1 = \alpha_2)$ & $(\psi_1 = \psi_2)$ is exclude in areas A0, A11, A12, A22, D1, D2, but is assigned to area A21 or D3;

(2) The configuration $(\alpha_2 = \alpha_3)$ & $(\psi_2 = \psi_3)$ is exclude in areas A12, A0, A21, A22, D2, D3, but is assigned to area A21 or D1.

Theorem 2. *The area A0 doesn't exist if*

(1) $\frac{\vec{F}_1}{\|\vec{F}_1\|} = \frac{\vec{F}_2}{\|\vec{F}_2\|}$, i.e. the forces have the same orientation,

(2) $\frac{\vec{F}_1}{\|\vec{F}_1\|} = -\frac{\vec{F}_2}{\|\vec{F}_2\|}$ and $F_1 \neq F_2$, i.e. the forces' orientations are opposite and they don't have the same strength.

The proof of Theorem 2 is provided in [39, Appendix F.3.1].

5.2. Forces applied inside the areas

From the areas properties exposed in Section 5 and PFS performed in Section 4.2, one can deduce that

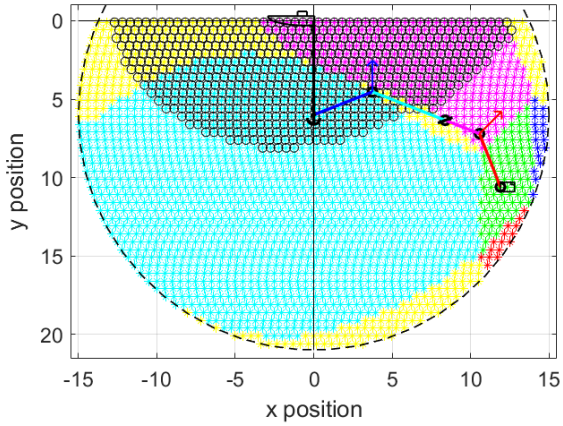

Figure 5: Areas for an umbilical with two sliding elements and an anchor. Green: A0. Blue: A11. Cyan: A12. Red: A21. Magenta: A22.Yellow: areas D. Black: area F where the umbilical cannot be stretched. Blue arrow : force $\vec{F}_1$. Red arrow: force $\vec{F}_2$.

- The PFD (9) with $i = 1$ is valid in areas A0, A11, A12, A22, D1;
- The PFD (9) with $i = 2$ is valid in areas A0, A12, A21, A22, D3;
- The PFD (10) is valid in area D2.

It can be deduced that T_1 does not exist in areas A21 and D3 , T_2 does not exist in area D2 and T_3 does not exist in areas A11 and D1.

Note also that

- Since element 1 is sliding in areas A0, A11, A12, the Theorem 1 is valid for $i = 1$;
- Since element 2 is sliding in areas A0, A21, A22, the Theorem 1 is valid for $i = 2$.

Moreover, the conditions described in Definition 2 must be respected for each sliding element.

In function of if the systems (9) and (10) exist, *i.e.* in function of the areas, the expressions of the forces T_1, T_2 and

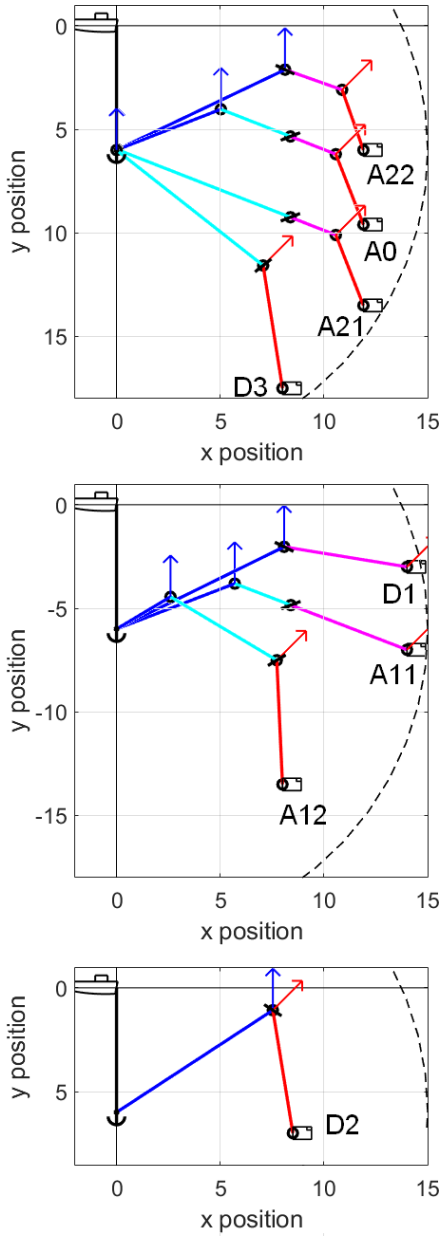

Figure 6: Illustration of the umbilical in all areas.

T_3 changed. Let's note $T_i^{S_j}$ for $i \in \{1,2,3\}$ and $j \in \{1,2\}$ the expression of T_1, T_2 and T_3 in function of the different cases exposed below. In all case, one has

$$F_{1xy} = \cos\left(\psi_{F1}\right) F_1 \tag{14}$$

$$F_{2xy} = \cos\left(\psi_{F2}\right) F_2. \tag{15}$$

$$T_i^{S_j} = \frac{T_{ixy}^{S_j}}{\cos\left(\psi_i\right)} \tag{16}$$

- **If not area D2**: the systems (9) is valid. Following steps described in [39, Appendix A.4], if $\cos\left(\alpha_1\right) \neq 0$ and/or $\cos\left(\alpha_3\right) \neq 0$, $\sin\left(\alpha_2 - \alpha_1\right) \neq 0$ and/or $\sin\left(\alpha_3 - \alpha_2\right)$, one gets $T_{1xy} = T_{1xy}^{S1}, T_{2xy} = T_{2xy}^{S1}$ and $T_{3xy} = T_{3xy}^{S1}$ where

$$T_{1xy}^{S1} = \begin{cases} 0 & \text{if A21 or D3,} \\ \frac{1}{\cos(\alpha_1)}\left(\cos\left(\alpha_2\right) T_{2xy}^{S1} + F_{1xy}\cos\left(\phi_1\right)\right) & \text{else,} \end{cases} \tag{17}$$

$$T_{3xy}^{S1} = \begin{cases} 0 & \text{if A11 or D1,} \\ \frac{1}{\cos(\alpha_3)}\left(\cos\left(\alpha_2\right) T_{2xy}^{S1} - F_{2xy}\cos\left(\phi_2\right)\right) & \text{else,} \end{cases} \tag{18}$$

with

$$T_{2xy}^{S1} = \begin{cases} -\frac{\sin(\phi_1-\alpha_1)}{\sin(\alpha_2-\alpha_1)} F_{1xy} & \text{if A0, A11, A12 or D1,} \\ -\frac{\sin(\phi_2-\alpha_3)}{\sin(\alpha_3-\alpha_2)} F_{2xy} & \text{if A21, A22 or D3.} \end{cases} \tag{19}$$

- **If area D2**: the systems (10) is valid. Following the steps described in [39, Appendix A.4.4], if $\cos\left(\alpha_1\right) \neq 0$ and $\sin\left(\alpha_3 - \alpha_1\right) \neq 0$, one has $T_{1xy} = T_{1xy}^{S2}$ and $T_{3xy} = T_{3xy}^{S2}$ where

$$T_{1xy}^{S2} = \frac{1}{\cos\left(\alpha_1\right)}\left(\cos\left(\alpha_3\right) T_{3xy}^{S2} + F_{\Sigma x}\right) \tag{20}$$

$$T_{3xy}^{S2} = \frac{F_{\Sigma x}\sin\left(\alpha_1\right) - F_{\Sigma y}\cos\left(\alpha_1\right)}{\sin\left(\alpha_3 - \alpha_1\right)} \tag{21}$$

and $T_{2xy}^{S2} = 0$ because doesn't exist.

In the case where $\alpha_3 = \alpha_1 + k_2\pi$ with $k_2 \in \mathbb{Z}$, one has $T_{3xy} = T_{1xy} = \frac{\sqrt{F_{\Sigma x}^2 + F_{\Sigma y}^2}}{2}$. If $\alpha_1 = s\frac{\pi}{2}$, one has $T_{3xy} = F_{\Sigma x}\frac{1}{\cos(\alpha_3)}$ and $T_{1xy} = s\left[\sin\left(\alpha_3\right) T_{3xy} + F_{\Sigma y}\right]$.

- **Particular cases:** if not area D2, in the case where $\alpha_1 = \alpha_2 + k_2\pi$ or $\alpha_3 = \alpha_2 + k_2\pi$ with $k_2 \in \mathbb{Z}$, one has respectively $T_{1xy} = T_{2xy} = \frac{F_{1xy}}{2}$ or $T_{3xy} = T_{2xy} = \frac{F_{3xy}}{2}$. Moreover, if $\alpha_1 = s\frac{\pi}{2}$ or $\alpha_3 = s\frac{\pi}{2}$, one has respectively $T_{2xy} = F_{1xy}\frac{\cos(\phi_1)}{\cos(\alpha_2)}$ and $T_{1xy} = sF_{1xy}\left[\tan\left(\alpha_2\right)\cos\left(\phi_1\right) + \sin\left(\phi_1\right)\right]$ or

  $T_{2xy} = F_{2xy}\frac{\cos(\phi_2)}{\cos(\alpha_2)}$ and

  $T_{3xy} = sF_{2xy}\left[\tan\left(\alpha_2\right)\cos\left(\phi_2\right) + \sin\left(\phi_2\right)\right]$.

Proves of all these expression can be found in [39, Appendix A].These systems will be used in next sections to solve the model of the umbilical.

6. Deduction of the current area

The method for deducing the current area can be summarized as follow. First, based on previous umbilical configuration (if known), the number of possible areas can be

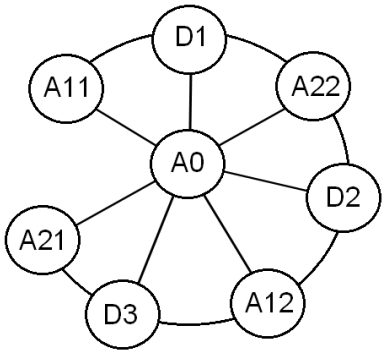

Figure 7: Graph of connection between areas.

reduced using the graph of areas exposed in Section 6.1. The system is then solved for all remaining areas, as it will be summarized in Section 6.2. If no solution can be found for an area, it is excluded. If only one area has a solution, it is automatically the current area. Otherwise, the system energy described in Section 6.3 is used to find the current solution as described in Section 6.4.

6.1. Graph of areas

When a sliding element moves on the cable, it comes in contact with a stop or becomes free again: the umbilical pass so from one configuration to another. One can define a graph of communication between the different areas, as summarizes in Figure 7. When some areas don't exist (see Table 1), the graph is cut off from the associated branches, but remains globally connected. Moreover, since an element cannot pass instantaneously from one stop to another without passing by a sliding phase, this graph is not fully-connected, *i.e.* the umbilical cannot always pass directly from any area to any other. Two areas directly connected are called neighbors.

This graph will be used to reduce the number of configurations to calculate to find the next shape of the umbilical.

6.2. Resolution of the model inside the areas

Due to their geometric and dynamic differences, each area requires its own mathematical resolution. Using a transformation of the referential and the simple geometrical shape of the umbilical in areas D1, D2 and D3, the solution of system (7) in theses areas can be found analytically. On the other hand, due to the high non-linearity of system (7), the model is too complex to be solved analytically in areas A0, A1 and A2: a theoretical solution is proposed along a numerical resolution. Details of these resolutions are given in Part IV.

6.3. Energy of the configuration

The principal of least action [14] argues that the static shape of the cable minimizes its potential energy. Therefore, this principal can be used to find the current solution by chosing the configuration with the lowest energy.

Let $E_p(\mathcal{A})$ be the energy of the configuration $\mathcal{A}$. E_p will be used in the Section 6.4 to compare results obtained in the different areas to find the actual umbilical configuration. In this section, we only consider configurations for which a solution can been found, *i.e.* where the position of B_1 and B_2 are known.

The movement of the element 1 are limited by the cable l_1 attached to the anchor $A = \begin{bmatrix} 0 & l_0 & 0 \end{bmatrix}^T$. If the cable l_1 were subjected only to the actions of $\vec{F}_1$, element 1 would slide since it came in contact with S, and then the part AS would behave like a pendulum, whose minimum potential energy $E_{p\min,1}$ is reached at the position $p_{E_{p\min,1}} = A + l_1 \frac{\vec{F}_1}{F_1}$, *i.e.* the point furthest from A in direction $\frac{\vec{F}_1}{F_1}$. Using A as reference, the energy $E_{p,1}$ of element 1 can so be expressed as

$$E_{p,1} = l_1 F_1 - \overrightarrow{AB_1}.\vec{F}_1 \tag{22}$$

In the same way, the element 2 is limited to the cable l_2 attached in S to the cable l_1. Following the same reasoning, the minimal energy $E_{p,2}$ of element 2 can so be expressed as

$$E_{p,2} = \left(l_1 + l_2\right) F_2 - \overrightarrow{AB_2}.\vec{F}_2 \tag{23}$$

with $\overrightarrow{AB_2} = \overrightarrow{AB_1} + \overrightarrow{B_1S} + \overrightarrow{SB_2}$. The energy of the system can so be expressed as

$$E_p = E_{p,1} + E_{p,2}. \tag{24}$$

6.4. Algorithm deduction of the area

The Part IV will provide theorems giving a solution to the system (7) if the ROV is inside a corresponding area. If not solution can be found for the current coordinate, then the ROV is not inside this area. However, it can happen that several solutions are found in different areas, and only one corresponds to the reality. This section allows to select the current solution between the several solution found.

Consider in this section that if a solution is possible in an area for the current coordinate, then this solution is found. The current configuration can be found using the following steps:

1. **Reduction of the number of areas possible:**
   (a) **Areas possible:** Table 1 defines the number of existing areas to be evaluated according to the elements on the umbilical.
   (b) **Areas neighbors:** when the area of the previous position is known, if the new coordinates, forces and cable length are close to the previous configuration, only the current zone and its neighbors as defined in Section 6.1 need to be evaluated.
2. **Evaluation of the solution in the different areas:** a solution is searched in each remaining area using Theorems exposed in Part IV, Sections 7 and 8.
3. **Selection of the areas:** if only one solution is found, this solution is the current configuration. Else, based on the principal of least action [14], the true solution is the one with the smallest energy E_p exposed in Section 6.3.

4. **Final test:** check if the solution is a submerged configuration, *i.e.* the coordinate y is positive for the points B_1, S and B_2.
5. **If not solution is found:** the system is in area F.

Remark 3. ***not solution is found****: in presence of at least one fixed element, sometime the umbilical cannot be stretched for some position of the ROV. In these conditions, the system (7) cannot find a solution and is considered inside area F. Example: element 1 is a fixed ballast pushing vertically with $l_1 > l_2$ (see [37]). The coordinate $(0, l_0, 0)$ requires the cable l_1 to be folded back to reach the position.*

Part IV
Resolution model in the areas

This part proposes a resolution of the model based on the assumptions and properties exposed in previous sections. Since the complete redaction of each solution for each area is very voluminous, we made the choice of presented in this paper only the methodology used and the main conditions to be met. The complete description and the proofs are provided in the extended version of this work in [39]. Reference to the appropriate theorem will always be specified in the text.

7. Resolution model in areas A0, A1 and A2

Due to the strong non-linearity of system (7), the model is too complex to be solved analytically in areas A0, A1 and A2, named here areas A. Thus, theorems exposed in this section proposes a theoretical solution and a numerical resolution of system (7).

7.1. Change of referential

To find a solution in the different areas, the system exposed in previous sections is easier to solve in others referential where some of these components become equal to zero.

In areas A0, A1 and A2, a simple around the vertical axis $O\vec{y}$ is used to obtain a referential $\mathcal{R}_j$ where the component $\psi_{F1|\mathcal{R}_j}$ or $\psi_{F2|\mathcal{R}_j}$ is equal to zero. The Definition 4 defines the referential $\mathcal{R}_0$, $\mathcal{R}_1$ and $\mathcal{R}_2$ respectively associated to the resolution of the system in the areas A0, A1 and A2.

Definition 4. *The referential $\mathcal{R}_j$ for $j \in \{0,1,2\}$ is defined as a rotation of the referential $\mathcal{R}$ around the axis $O\vec{y}$ of an angle $\mu_j = atan2\left(F_{jz|\mathcal{R}}, F_{jx|\mathcal{R}}\right)$ if $j \in \{1,2\}$, $\mu_0 = atan2\left(F_{1z|\mathcal{R}}, F_{1x|\mathcal{R}}\right)$ if $j = 0$. Let $M_y^{\mathcal{R}}\left(\mu_j\right)$ be the rotation matrix allowing to pass from $\mathcal{R}$ to $\mathcal{R}_j$. Note that*

(1) the lengths l_{11}, l_{12}, l_{21}, l_{22} are unaffected by the change of referential;

(2) the coordinate of the ROV can be evaluated such that $\begin{bmatrix} x & y & z \end{bmatrix}_{\mathcal{R}_j}^T = M_y\left(\mu_j\right) \begin{bmatrix} x & y & z \end{bmatrix}_{\mathcal{R}}^T$.

7.2. Additional notations

For a referential $\mathcal{R}_i$, let's define the energy of the system (7)

$$\boldsymbol{E}_{\mathcal{R}_i} = \Big\| \overrightarrow{AB}_{1|\mathcal{R}_i} + \overrightarrow{B_1B_2}_{|\mathcal{R}_i} + \overrightarrow{B_2R}_{|\mathcal{R}_i} - \begin{bmatrix} x & (y - l_0) & z \end{bmatrix}_{\mathcal{R}_i}^T \Big\|^2 \tag{25}$$

This energy will be used to solve the umbilical model.

Since a solution will be required to be evaluated in each area, the different angles and lengths are grouped in a set of parameters expressed in Definition 5.

Definition 5. *Let's define the area $A_m \in \{A0, A11, A12, A21, A22\}$ and note $\mathcal{R}_m$ the referential associated to area A_m as defined in Definition 4. For $(x, y, z) \in \bar{C}_{A,r}$, let $\mathcal{L}_{\alpha,\psi,l}^{A_m}\left(\alpha_{1|\mathcal{R}_k}\right)$ be the set of parameters*

$$\mathcal{L}_{\alpha,\psi,l}^{A_m}\left(\alpha_{1|\mathcal{R}_m}\right) = \Big\{ \alpha_{1|\mathcal{R}_k}, \alpha_{2|\mathcal{R}_m}, \alpha_{3|\mathcal{R}_k}, \psi_{1|\mathcal{R}_m}, \psi_{2|\mathcal{R}_k}, \psi_{3|\mathcal{R}_m}, l_{11}, l_{12}, l_{21}, l_{22} \Big\} \tag{26}$$

evaluated for the angle $\alpha_{1|\mathcal{R}_k}$ and $(x, y, z)_{\mathcal{R}_m}$ using respectively

(1) [39, Theorem 4] for area A11,
(2) [39, Theorem 5] for area A12,
(3) [39, Theorem 6] for area A21,
(4) [39, Theorem 7] for area A22,
(5) For area A0, [39, Theorem 8] if $\psi_{F2|\mathcal{R}_0} = 0$, [39, Theorem 9] else.

Let also note $\boldsymbol{E}_{\mathcal{R}_k}\left(\mathcal{L}_{\alpha,\psi,l}^{A_m}\right)$ the evaluation of (25) using parameters inside $\mathcal{L}_{\alpha,\psi,l}^{A_m}$.

In order to lighten notations, $\mathcal{L}_{\alpha,\psi,l}^{A_m}\left(\alpha_{1|\mathcal{R}_m}\right)$ will be written $\mathcal{L}_{\alpha,\psi,l}^{A_m}$ in the next sections of the paper.

Theorems exposed in Definition 5 provide sets of parameters $\mathcal{L}_{\alpha,\psi,l}^{A_m}$ which will be used in Theorem 3 to solve the system in areas A. Even if theses theorems are provided in [39], more details and conditions used in these theorems will be provided in the next sections.

7.3. Resolution of the system in areas A

Due to the strong non-linearity of system (7) and in opposite to areas D described in Section 8, the model is too complex to be solved analytically in areas A. The theoretical solution can however be expressed, and a numerical resolution is proposed to find a solution to the system. These two aspects are described in Theorem 3.

Theorem 3. *Consider an area $A_m \in \{A0, A11, A12, A21, A22\}$, its associated referential $\mathcal{R}_m$ and the set of parameters $\mathcal{L}_{\alpha,\psi,l}^{A_m}\left(\alpha_{1|\mathcal{R}_m}\right)$ evaluated for an angle $\alpha_{1|\mathcal{R}_m}$ as defined in Definition 5. For the coordinate $(x, y, z) \in \bar{C}_{A,r}$, a solution of system (7) exists in the area A_m if there exists an angle*

$\alpha_{1|\mathcal{R}_m} \in [-\pi, \pi]$ *such as the associated* $\mathcal{L}^{A_m}_{\alpha,\psi,l}\left(\alpha_{1|\mathcal{R}_m}\right)$ *guarantee*

$$E^{A_m}_{\min} \leq \eta \tag{27}$$

where

$$E^{A_m}_{\min} = \min_{\substack{\alpha_{1|\mathcal{R}_m} \in [-\pi,\pi] \\ \mathcal{L}^{A_m}_{\alpha,\psi,l}\left(\alpha_{1|\mathcal{R}_m}\right) \neq \emptyset}} \boldsymbol{E}_{\mathcal{R}_k}\left(\mathcal{L}^{A_m}_{\alpha,\psi,l}\left(\alpha_{1|\mathcal{R}_m}\right)\right). \tag{28}$$

and with $\eta = 0$ *in theoretical case,* $\eta \geq 0$ *a chosen parameter for numerical resolution.*

If a solution exist, this solution $S^{A_m}_{\alpha,\psi,l}$ *can be expressed as*

$$S^{A_m}_{\alpha,\psi,l} = \left\{ \mathcal{L}^{A_m}_{\alpha,\psi,l}\left(\alpha_{1|\mathcal{R}_m}\right) \mid \boldsymbol{E}_{\mathcal{R}_m}\left(\mathcal{L}^{A_m}_{\alpha,\psi,l}\left(\alpha_{1|\mathcal{R}_m}\right)\right) = E^{A_m}_{\min}, \; \mathcal{L}^{A_m}_{\alpha,\psi,l}\left(\alpha_1\right) \neq \emptyset, \; \forall \alpha_{1|\mathcal{R}_m} \in [-\pi, \pi] \right\}. \tag{29}$$

In theory, the unique solution of the system (7) is $\alpha_{1|\mathcal{R}_m}$ solution of (25), which is equivalent to solve (27) with $\eta = 0$ in Theorem 3.

The proof of Theorem 3 is connected to the proofs of Theorems 4,5,6,7,8 and 9 in [39] which will be exposed in the next sections, each one for a specific areas.

7.4. Length calculation

The calculation of the length of cables l_{11}, l_{12}, l_{21} and l_{22} can be performed if the angles α_i and ψ_i for $i \in \{1, 2, 3\}$ are known. In function of the umbilical configuration, some lengths are already known, see Section 5. Note that the umbilical lengths are identical in all references, so they can be calculated with the angles of any referential.

The calculation is described in [39, Section 6.4].

7.5. Solution in Area A1

Theorems 4 and 5 in [39] proposes a set of parameters $\mathcal{L}^{A11}_{\alpha,\psi,l}\left(\alpha_{1|\mathcal{R}_1}\right)$ and $\mathcal{L}^{A12}_{\alpha,\psi,l}\left(\alpha_{1|\mathcal{R}_1}\right)$, possibly solution in area A11 in referential $\mathcal{R}_1$.

Based on properties made in Section 5 and Definition 2 for the sliding element 1, and the element 2 in contact with S or R, the Definition 6 provides conditions which must be satisfied to guarantee the physical and geometrical feasibility of solutions in areas A11 and A12. Theses conditions are applied in Theorem 4 and 5 in [39].

Definition 6. *From Definition 2, a set of parameters* $\mathcal{L}^{A11}_{\alpha,\psi,l}$ *or* $\mathcal{L}^{A12}_{\alpha,\psi,l}$ *is a possible solution of system (7) in respectively area A11 or area A12 iff the following condition* C^{A1} *is respected*

$$C^{A1} = \left(C^{A1}_1\right) \& \left(C^{A1}_2\right) \& \left(C^{A1}_3\right) \& \left(C^{A1}_4\right) \tag{30}$$

with

$$C^{A1}_1 = \left(0 \leq l_{11} \leq l_1\right) \& \left(0 \leq l_{12} \leq l_1\right) \tag{31}$$

$$C^{A1}_2 = \left(T^{S1}_{1|\mathcal{R}_1} > 0\right) \& \left(T^{S1}_{2|\mathcal{R}_1} > 0\right) \& \left(T^{S1}_{3|\mathcal{R}_1} \geq 0\right) \tag{32}$$

$$C^{A1}_3 = \left(\vec{F}_1.\overrightarrow{AB_1} > 0\right) \& \left(\vec{F}_1.\overrightarrow{B_1S} < 0\right) \tag{33}$$

$$C^{A1}_4 = \begin{cases} True & \text{if element 2 is fixed or } l_2 = 0, \\ \left(\vec{F}_2.\overrightarrow{SB_2} > 0\right) & \text{else if A11} \\ \left(\vec{F}_2.\overrightarrow{B_2R} < 0\right) & \text{else if A12} \end{cases} \tag{34}$$

where $T^{S1}_{1|\mathcal{R}_1}$, $T^{S1}_{2|\mathcal{R}_1}$ *and* $T^{S1}_{3|\mathcal{R}_1}$ *are evaluated using (16).*

7.6. Solution in area A2

The Theorems 6 and 7 in [39] propose a set of parameters $\mathcal{L}^{A21}_{\alpha,\psi,l}\left(\alpha_{1|\mathcal{R}_2}\right)$ and $\mathcal{L}^{A22}_{\alpha,\psi,l}\left(\alpha_{1|\mathcal{R}_2}\right)$, possibly solution in areas A21 and A22 in referential $\mathcal{R}_2$.

Like for Definition 6 in area A1, the Definition 7 provides conditions for areas A21 and A22. Theses conditions are applied in Theorems 6 and 7 in [39].

Definition 7. *From Definition 2, a set of parameters* $\mathcal{L}^{A21}_{\alpha,\psi,l}$ *or* $\mathcal{L}^{A22}_{\alpha,\psi,l}$ *is a possible solution of system (7) in respectively area A21 or area A22 iff the following condition* C^{A2} *is respected*

$$C^{A2} = \left(C^{A2}_1\right) \& \left(C^{A2}_2\right) \& \left(C^{A2}_3\right) \& \left(C^{A2}_4\right) \tag{35}$$

with

$$C^{A2}_1 = \left(0 \leq l_{21} \leq l_2\right) \& \left(0 \leq l_{22} \leq l_2\right) \tag{36}$$

$$C^{A2}_2 = \left(T^{S1}_{1|\mathcal{R}_1} \geq 0\right) \& \left(T^{S1}_{2|\mathcal{R}_1} > 0\right) \& \left(T^{S1}_{3|\mathcal{R}_1} > 0\right) \tag{37}$$

$$C^{A2}_3 = \left(\vec{F}_2.\overrightarrow{SB_2} > 0\right) \& \left(\vec{F}_2.\overrightarrow{B_2R} < 0\right) \tag{38}$$

$$C^{A2}_4 = \begin{cases} True & \text{if element 1 is fixed,} \\ \left(\vec{F}_1.\overrightarrow{B_1S} < 0\right) & \text{else if A21} \\ \left(\vec{F}_1.\overrightarrow{AB_1} > 0\right) & \text{else if A22} \end{cases} \tag{39}$$

where $T^{S1}_{1|\mathcal{R}_1}$, $T^{S1}_{2|\mathcal{R}_1}$ *and* $T^{S1}_{3|\mathcal{R}_1}$ *are evaluated using (16).*

7.7. Solution in Area A0

The Theorems 8 and 9 in [39] propose a set of parameters $\mathcal{L}^{A0}_{\alpha,\psi,l}\left(\alpha_{1|\mathcal{R}_0}\right)$, possibly solution in area A0 in referential $\mathcal{R}_0$. Like for Definition with area A1, the Definition 8 provides conditions in area A0. Theses conditions are applied in Theorems 8 and 9 in [39].

Definition 8. *From Definition 2, a set of parameters* $\mathcal{L}^{A0}_{\alpha,\psi,l}$ *is a possible solution of system (7) in area A0 iff the following condition* C^{A0} *is respected*

$$C^{A0} = \left(C^{A1}_1\right) \& \left(C^{A2}_1\right) \& \left(C^{A2}_2\right) \& \left(C^{A0}_1\right) \& \left(C^{A0}_2\right) \tag{40}$$

with

$$C_1^{A0} = \left(\vec{F}_1.\overrightarrow{AB_1} > 0\right) \& \left(\vec{F}_1.\overrightarrow{B_1S} < 0\right) \quad (41)$$

$$C_2^{A0} = \left(\vec{F}_2.\overrightarrow{SB_2} > 0\right) \& \left(\vec{F}_2.\overrightarrow{B_2R} < 0\right) \quad (42)$$

where $T^{S1}_{1|\mathcal{R}_0}$, $T^{S1}_{2|\mathcal{R}_0}$ *and* $T^{S1}_{3|\mathcal{R}_0}$ *are evaluated using (16).*

8. Resolution model in areas D1, D2 and D3

Using a transformation of the referential, the solution of system (7) in areas D (D1, D2 and D3) can be found analytically. For that, the referential is transformed using a translation and three rotations of $\mathcal{R}$, described in the subsection 8.2.

8.1. Force applied at stop S

Let's define $\vec{F}_{S|\mathcal{R}} = \begin{bmatrix} F_{Sx|\mathcal{R}} & F_{Sy|\mathcal{R}} & F_{Sz|\mathcal{R}} \end{bmatrix}^T$ the force at the stop S expressed as

$$\vec{F}_{S|\mathcal{R}} = \vec{F}_{1|\mathcal{R}} \quad \text{in area D1} \quad (43)$$

$$\vec{F}_{S|\mathcal{R}} = \vec{F}_{\Sigma|\mathcal{R}} = \vec{F}_{1|\mathcal{R}} + \vec{F}_{2|\mathcal{R}} \quad \text{in area D2} \quad (44)$$

$$\vec{F}_{S|\mathcal{R}} = \vec{F}_{2|\mathcal{R}} \quad \text{in area D3.} \quad (45)$$

This force will be used in the resolution of the model.

8.2. Change of referential $\mathcal{R}_D$

In the areas D, all the elements are in contact with a stop. Thus, the umbilical between the anchor and the ROV becomes the triangle ASR with $AS = l_1$ and $SR = l_2$. Moreover, there is a referential where the triangle ASR and all forces applied on A, S and R can be expressed in a 2D plan $\left(O\vec{x}\vec{y}\right)$. This referential, named $\mathcal{R}_D$, can be obtained by performing a translation and three rotation of the referential $\mathcal{R}$, as illustrated in Figure 8. The Definition 9 defines the referential $\mathcal{R}_D$ associated to the resolution of the system in the areas D1, D2 and D3.

Definition 9. *The referential $\mathcal{R}_D$ is defined as a translation and three rotations of the referential $\mathcal{R}$. The vector of coordinate $X_{\mathcal{R}} = \begin{bmatrix} x & y & z \end{bmatrix}^T_{\mathcal{R}}$ and forces $\vec{F}_{i|\mathcal{R}_D}$ $\forall i \in \{1, 2, S\}$ can be expressed in $\mathcal{R}_D$ such as*

$$X_{\mathcal{R}_D} = M_D\left(X_{\mathcal{R}} - T_{\mathcal{R}}\right) \quad (46)$$

$$\vec{F}_{i|\mathcal{R}_D} = M_D\vec{F}_{i|\mathcal{R}} \quad (47)$$

$$M_D = M_x\left(\mu_{D(3)}\right) M_y\left(\mu_{D(2)}\right) M_z\left(\mu_{D(1)}\right) \quad (48)$$

where

$$T_{\mathcal{R}} = \begin{bmatrix} 0 & l_0 & 0 \end{bmatrix}^T_{\mathcal{R}} \quad (49)$$

$$X_{\mathcal{R}_{D(1)}} = X_{\mathcal{R}} + T_{\mathcal{R}} \quad (50)$$

$$X_{\mathcal{R}_{D(2)}} = M_z\left(\mu_{D(1)}\right) X_{\mathcal{R}_{D(1)}} \quad (51)$$

$$\vec{F}_{i|\mathcal{R}_{D(3)}} = M_y\left(\mu_{D(2)}\right) M_x\left(\mu_{D(1)}\right) \vec{F}_{i|\mathcal{R}} \quad (52)$$

$$\mu_{D(1)} = -atan2\left(y_{\mathcal{R}_{D(1)}}, x_{\mathcal{R}_{D(1)}}\right) \quad (53)$$

$$\mu_{D(2)} = atan2\left(z_{\mathcal{R}_{D(2)}}, x_{\mathcal{R}_{D(2)}}\right) \quad (54)$$

$$\mu_{D(3)} = -atan2\left(F_{Sz|\mathcal{R}_{D(3)}}, F_{Sy|\mathcal{R}_{D(3)}}\right) \quad (55)$$

8.3. Solution in areas D

Due to the change of referential $\mathcal{R}_D$, the system (7) can be expressed in two dimensions with the following general form

$$x_{\mathcal{R}_D} = l_1\cos(\gamma) + l_2\cos(\beta) \quad (56)$$

$$y_{\mathcal{R}_D} = l_1\sin(\gamma) + l_2\sin(\beta). \quad (57)$$

where $\{\gamma, \beta\}$ are respectively equal to $\{\alpha_1, \alpha_2\}$ in area D1, $\{\alpha_1, \alpha_3\}$ in area D2, and $\{\alpha_2, \alpha_3\}$ in area D3. A first set of solutions can so be defined using only the geometrical properties of the system, described in [39, Theorem 11]. Since the solution found is not unique, the dynamical properties are added to find the current solution, as described in Theorem 4.

Theorem 4. *Consider the system (7) with $(x, y, z) \in \bar{\mathcal{C}}_{A,r}$ and is inside the area D1, D2 or D3. Considering the assumptions A1 to A8. In referential $\mathcal{R}_D$, let's define $L_{\gamma,\beta} = \{\gamma, \beta\}$ the set of solution defined in [39, Theorem 11]. Then*

(1) In area D1, $\alpha_{1|\mathcal{R}_D} = \gamma$, $\alpha_{2|\mathcal{R}_D} = \beta$, $\alpha_{3|\mathcal{R}_D} = 0$, $l_{11} = l_1$, $l_{12} = 0$, $l_{21} = l_2$, $l_{22} = 0$, where $(\gamma, \beta) \in L_{\gamma,\beta}$ and respect the conditions $\boldsymbol{E}_{\mathcal{R}} = 0$ and

$$\left(T^{S1}_{1|\mathcal{R}_D} > 0\right) \& \left(T^{S1}_{2|\mathcal{R}_D} > 0\right) \quad (58)$$

$$\left(\vec{F}_1.\overrightarrow{AS} > 0\right) \quad \textit{if element 1 is not fixed} \quad (59)$$

$$\left(\vec{F}_2.\overrightarrow{SR} > 0\right) \quad \textit{if element 2 is not fixed} \quad (60)$$

(2) In area D2,$\alpha_{1|\mathcal{R}_D} = \gamma$, $\alpha_{2|\mathcal{R}_D} = 0$, $\alpha_{3|\mathcal{R}_D} = \beta$, $l_{11} = l_1$, $l_{12} = 0$, $l_{21} = 0$, $l_{22} = l_2$, where $(\gamma, \beta) \in L_{\gamma,\beta}$ and respect the conditions $\boldsymbol{E}_{\mathcal{R}} = 0$ and

$$\left(T^{S1}_{1|\mathcal{R}_D} > 0\right) \& \left(T^{S1}_{3|\mathcal{R}_D} > 0\right) \quad (61)$$

$$\left(\vec{F}_1.\overrightarrow{AS} > 0\right) \quad \textit{if element 1 is not fixed} \quad (62)$$

$$\left(\vec{F}_2.\overrightarrow{SR} < 0\right) \quad \textit{if element 2 is not fixed} \quad (63)$$

(3) In area D3, $\alpha_{1|\mathcal{R}_D} = 0$, $\alpha_{2|\mathcal{R}_D} = \gamma$, $\alpha_{3|\mathcal{R}_D} = \beta$, $l_{11} = 0$, $l_{12} = l_1$, $l_{21} = 0$, $l_{22} = l_2$, where $(\gamma, \beta) \in L_{\gamma,\beta}$ and respect the conditions $\boldsymbol{E}_{\mathcal{R}} = 0$ and

$$\left(T^{S2}_{2|\mathcal{R}_D} > 0\right) \& \left(T^{S2}_{3|\mathcal{R}_D} > 0\right) \quad (64)$$

$$\left(\vec{F}_1.\overrightarrow{AS} < 0\right) \quad \textit{if element 1 is not fixed} \quad (65)$$

$$\left(\vec{F}_2.\overrightarrow{SR} < 0\right) \quad \textit{if element 2 is not fixed} \quad (66)$$

with $\overrightarrow{AS} = \overrightarrow{AB_1} + \overrightarrow{B_1S}$ *and* $\overrightarrow{SR} = \overrightarrow{SB_2} + \overrightarrow{B_2R}$.

The proof of Theorem 4 are provided in [39, Appendix G.3].

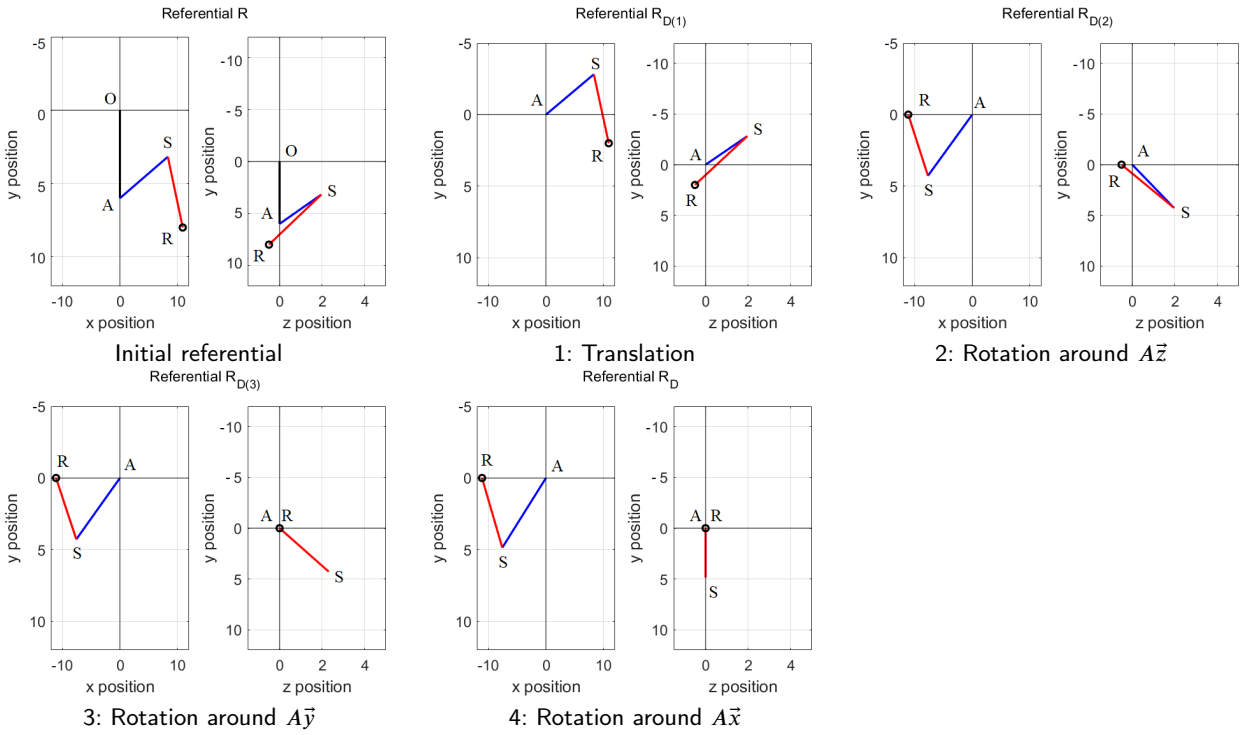

Figure 8: Transformations to pass from the referential $\mathcal{R}$ to the referential $\mathcal{R}_D$. After four transformations, one observes the part ASR of the umbilical is contained inside the plan $\left(O\vec{x}\vec{y}\right)_{\mathcal{R}_D}$.

9. Numerical resolution

To find a solution to Theorem 3 of Section 7, we propose to solve it numerically using a global optimization. Note that a global optimization is required because the system has a lot of local minimum due to the presence of cos, sin and tan functions. In this section, some comments are made to reduce the computation time and outline some numerical problems which can occur.

1) In a numerical resolution, all conditions of form $X = 0$ must be replaced by $|X| < \epsilon$ where $1 \gg \epsilon > 0$. In our simulations, on takes $\epsilon = 0.01$.

2) The Theorem 3 induces to test all $\alpha_1 \in \Lambda$ with $\Lambda = [-\pi, \pi]$, which can induce a long computation time. However, it can be observed that

- A global research on $\Lambda = [-\pi, \pi]$ is required only for the first estimation of the system and a first value of α_1. Then, if the new coordinates, forces and cable length are close to the parameters of the previous, Λ can be reduced to an interval $\Lambda_{k+1} = \alpha_1(k) + \omega$ where $\omega = \left[-\frac{\pi}{12}, \frac{\pi}{12}\right]$ or smaller, close to the value $\alpha_1(k)$ found at the previous iteration k. Note that in the case where the solution was found in areas A21 or D3 where $l_{11} = 0$ and so α_1 doesn't exist, the optimization must be done for parameter α_2, because the value of α_1 can change abruptly when the area changes.
- Since the calculation for each α_1 are independent, these ones can be made in parallel.

3) In the numerical resolution, a solution of Theorem 3 is valid if its energy $E_{\min}^{A_m}$ is bellow a defined threshold $\eta \geq 0$. The choice of η can be tricky because a too high threshold can admit a solution in a zone where there should be none, and a too small threshold can exclude solution where numerical rounding would be too penalizing. η must be found empirically. In our simulation, we choose $\eta = 0.1$.

4) The method is very sensible to small the variation of α_1. A final accuracy of $\delta\alpha_1 = 0.0001°$ is recommend for simulation. In our simulations, three optimizations' step were performed: a first loop with an accuracy of $\delta\alpha_1 = 0.01$ is performed where all local minimal are kept regardless of η, then a second research around these local minimal with a step of $\delta\alpha_1 = 0.001$, then a last step where the minimal energy $E_{\min}^{A_m}$ and the threshold η are considered.

Part V
Simulation, results, conclusion

10. Simulations and results

10.1. Examples of system

Simulations have been performed with Matlab R2019b, using the tool "parfor" with 4 workers (maximum of the computer used) to obtain a low parallelization of the operations.

In addition to the example in Figures 5 and 6, nine examples of umbilical shape are illustrated in Figure 9 to show the possibilities and performances of the model.

Sub-Figures 9**(1)** and **(2)** propose an exploration close to the surface to avoid hull or underwater cavern ceiling. Sub-Figures 9**(4)** and **(5)** propose an exploration close to the seabed to avoid and dive between obstacles such as rocks. Sub-Figure 9**(6)** adds presence of underwater current, with a more realistic representation of sub-Figure 9**(4)** where the anchor can move (here the "anchor" is a heavy ballast in the model). This sub-figure illustrates also the main advantage of using sliding element instead of fixed: the area marked C* is inaccessible with a fixed ballast, but not with a sliding ballast. Sub-Figures 9**(3)** and **(9)** use a motorized element to create a vertical force, allowing to explore a cavern in the wall. Finally, sub-Figures 9**(7)** and **(8)** show illustration of area A0 with theoretical forces, not necessarily useful or realistic in practice, but showing the performance of the proposed model.

The configurations expressed in sub-Figures 9**(1)**, **(2)**, **(4)**, **(5)** and **(6)** have been tested experimentally in pool, see Figure 10. The shape of the umbilical was also tested at sea with a cable of 15 m with (1) two ballasts, (2) one ballast and a buoy. Sliding elements were performed using pulley with a neutral buoyancy. The umbilical used was a Fathom ROV Tether[1] with a single twisted-pair network cable, 4mm in diameter. This thin cable allows very good flexibility. Conversely, the same model with a four-pair network cable and a 10mm diameter was too rigid to achieve good results, even if umbilical management was possible. A video of the first configuration is available at https://www.youtube.com/watch? v=BfcRRaSGlJA. Results are described in Section 10.2.1.

10.2. Results and comments

10.2.1. Experiments results and comparison with previous models

Experimental results of configurations illustrated in Figure 9**(1)**, **(4)** and **(6)** are described in [37, 38]. Experimental results of configurations Figure 9**(2)** and **(5)** are described in [36]. In these previous works, each configuration had its own model, and their accuracy with reality has already been demonstrated. Tests have been performed in a pool of size 3 m × 4 m, with a depth of 3 m (not the pool where the photos were taken).

The new general model allows to find the same geometrical results as the previous works. The main difference is that the computation time is lower than for the previous models, as the assumptions made in these works allow simplifications that permit analytical resolution in all cases. It should be noted, however, that most of these models cannot take into account the presence of horizontal underwater currents or three-dimensional cases, and testing a new configuration would require redoing a complete study of the system. Conversely, the new general model enables us to calculate the cable shape for all configurations using one or two elements.

10.2.2. A third element

A third element between R and the ROV can be considered if, like the anchor, its position relative to the ROV remains fixed: its coordinates become those of the ROV in the calculations. This can be used to offset the cable attachment point, for example with a buoy or ballast, for better diving between rocks.

10.2.3. Observations made

A hierarchy has been observed between the different areas. First, if area A0 exists, this configuration always has priority over all other areas. Then, the areas A (A11, A12, A21 and A22) have priority over the areas D (D1, D2 and D3). We tested this hierarchy by prioritizing one solution over another, and using the system's energy in case of conflict between two solutions inside areas A or inside areas D. The same results were observed as those obtained using only the system's energy. Couple with graph theory, this hierarchy could be an effective method to solve computation time by testing first area A0, then areas A if no solution is found and finally areas D. Unfortunately, no theoretical study has been found to prove this hierarchy, thus there is no guarantee of the reliability of this method.

10.2.4. Computation time

The computation time is proportional to the number of areas to evaluate, thus we consider here configurations with two sliding elements, *i.e.* with the greater number of areas. Between each iteration, a displacement of 0.5m for a cable of $L = 15$m is performed. The system is solved using resolution described in Part IV.

After the first estimation of the system, the computation time at each iteration is between 0.8s and 1.2s with Matlab R2019b and its tool "parfor" with 4 workers. This computation time is too long for a real-time implementation. A possible way to further speed up the real-time performance of our implementation would be transpiling the Matlab code to C++ or Python. An implementation on GPU to obtain a better calculation parallelization would strongly improve computation time. Other methods of resolution, for example finite element (with only three elements), could also be proposed. However, it can be noted that the computation time of our method is completely independent of the length

[1] https://bluerobotics.com/store/cables-connectors/cables/fathom-rov-tether-rov-ready/

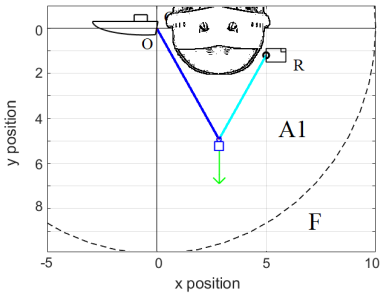

(1) 1 sliding ballast
$\vec{F}_1 = [0,\ 1,\ 0]^T$
$l_0 = 0,\ l_1 = 10$

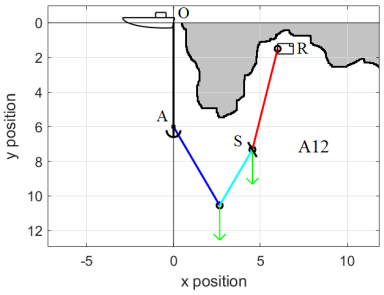

(2) 2 sliding ballasts
$\vec{F}_1 = [0,\ 1,\ 0]^T,\ \vec{F}_2 = \frac{1}{2}\vec{F}_1,$
$l_0 = 6,\ l_1 = l_2 = 10$

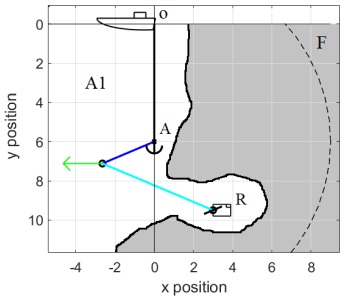

(3) 1 sliding vertical thruster
$\vec{F}_1 = [-1,\ 0,\ 0]^T$
$l_0 = 6,\ l_1 = 9$

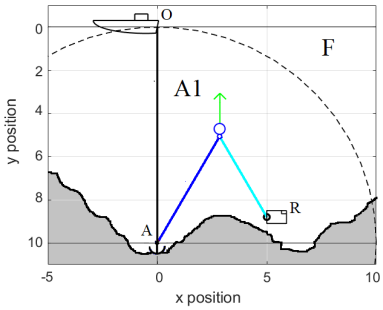

(4) 1 sliding buoy
$\vec{F}_1 = [0,\ -1,\ 0]^T$
$l_0 = l_1 = 10$

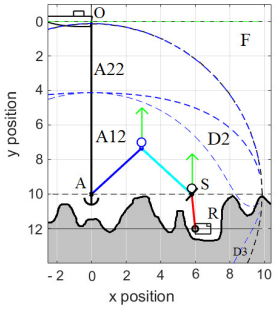

(5) 2 sliding buoys
$\vec{F}_1 = [0,\ -1,\ 0]^T,\ \vec{F}_2 = 2\vec{F}_1$
$l_0 = 10,\ l_1 = 6,\ l_2 = 4$

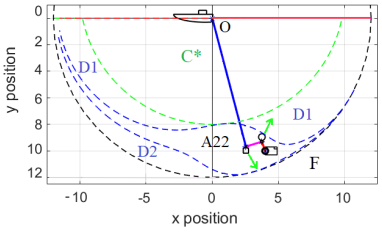

(6) 1 fixed or sliding ballast, 1 sliding buoy, both with horizontal underwater current
$\vec{F}_1 = [0.5,\ 2,\ 0]^T,\ \vec{F}_2 = [0.5,\ -1,\ 0]^T$
$l_0 = 0,\ l_1 = 10,\ l_2 = 2$
C*= F if fixed ballast,
C*=A11 if sliding ballast

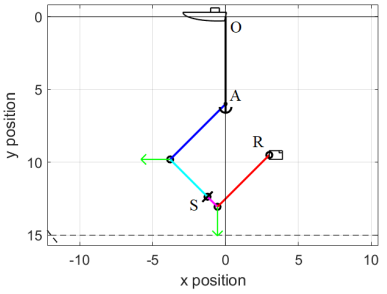

(7) Theoretical configuration to illustrate A0 with opposing forces
$\vec{F}_1 = [-1,\ 0,\ 0]^T,\ \vec{F}_2 = [0,\ 1,\ 0]^T$
$l_0 = 6,\ l_1 = 9,\ l_2 = 6$

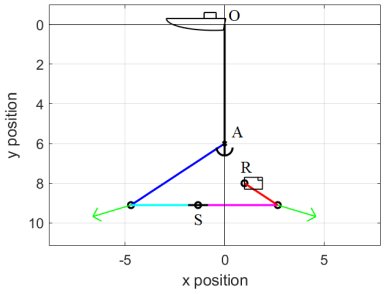

(8) Theoretical configuration to illustrate A0 with opposing forces
$\vec{F}_1 = [-1,\ 0.3,\ 0]^T,\ \vec{F}_2 = [1,\ 0.3,\ 0]^T$
$l_0 = 6,\ l_1 = 9,\ l_2 = 6$

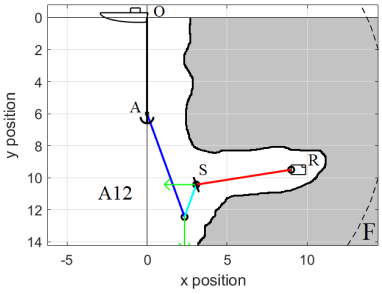

(9) 1 sliding ballast, 1 fixed vertical thruster
$\vec{F}_1 = [0,\ 1,\ 0]^T,\ \vec{F}_2 = [-3,\ 0,\ 0]^T$
$l_0 = 6,\ l_1 = 9,\ l_2 = 6$

Figure 9: Example of configurations possibles obtained with the proposed model. Areas possible/visible are noted in the illustrations. Grey areas: theoretical obstacles to illustrate the main interest of the illustrated configuration. In subfigure (1)-(3), only area A1 exist (with A11 = A12 because only one element). Note that it's the ratio between two lengths or distances that matters, not the unit.

of the umbilical, unlike the finite element methods where the computation increases linearly with the number of nodes, and hence the length of the cable (as in [13]).

10.3. Limits of the method and overview

The model provides a good vision of the system in offline, allowing to build a umbilical equipment and observe its behavior. However, the model has some limitations.

First, as already discussed in Section 10.2.4, the computation time is actually the major weakness of our method. Suggestions for improvement have been made in Section 10.2.4.

The method is also limited to two elements: except the case exposed in Section 10.2.2, each element added would multiple the number of possible areas by three, making the solution too complex to find and/or non-efficient in terms of the computation time.

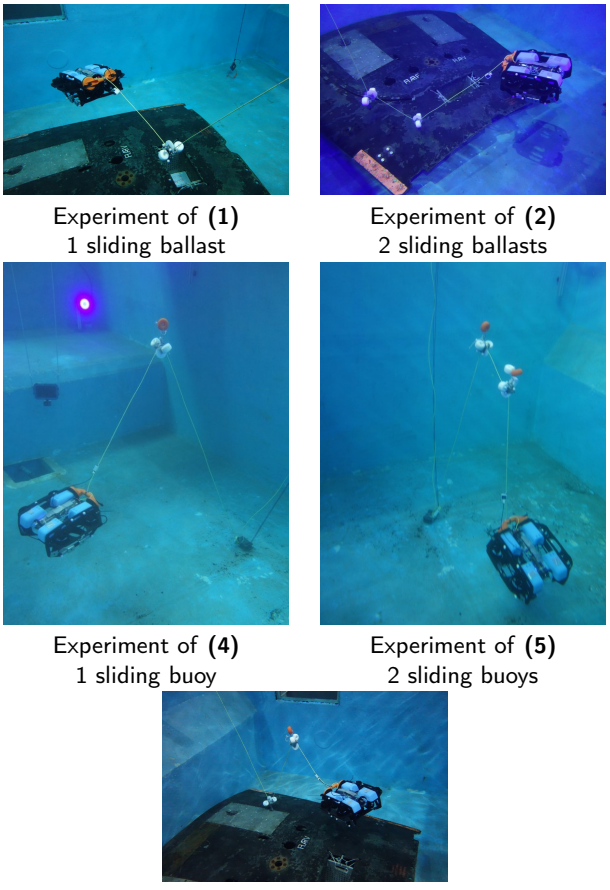

Experiment of **(1)** 1 sliding ballast

Experiment of **(2)** 2 sliding ballasts

Experiment of **(4)** 1 sliding buoy

Experiment of **(5)** 2 sliding buoys

Experiment of **(6)** : 1 sliding ballast and 1 sliding buoy

Figure 10: Configurations exposed in Figure 9 tested in pools. A robot BlueROV2 is used for the experiements.

More elements could be added with an more efficient computation time by

- Use of a less general model, for example in 2D and/or with elements having a specific orientation, or using more fixed elements, like in [37, 36].
- Changing the method of resolution: solving the problem with theorems exposed in Part IV may be heavy for some areas. By retaining assumption and properties proven in Part II, another type of resolution such as finite-element might be more efficient.

It can however be remark that in practice, install more than two elements can be useless or more unstable.

Another practical problem is knowing the forces applied to the elements. While the forces of weight, buoyancy or motorization are easy to obtain, it is more complex to know the forces of underwater currents or other external factors in practice. However, this problem is common to all umbilical models.

It can also be noted that the system is solved with quasi-static equilibrium hypotheses. Solutions to respect the hypotheses of quasi-static have been proposed in Section 4.2 and a resolution of the system in dynamic will be the subject of future studied.

10.4. Comparison with some existing models

This section compares our method with several open-source ROV models with tether.

[18, 17] proposes a position-based models used in a larger simulator of underwater environment. The tether model is designed for visual simulations: it is visually realistic, but does not correspond to real physical value as it does not deal with the forces applied to the cable. These simplifications enable it to have a lower computation time than our method, and to model an umbilical moving freely underwater without our assumption A3. However, it cannot take into account additional elements such as ballast unlike our study. Furthermore, no experiments have been carried out to verify the validity of the model, although some experiments have been performed with our model.

In [41], the tether has been modeled using a lumped-mass approach. An external force can be considered on each node, which would allow to consider the forces of external elements as ballast, although this case has not been studied. However, taking into account sliding forces on the cable would be more complex, and the computation time increases linearly with the number of nodes, i.e. with the tether's length in opposite with our study . Finally, the impact on the ROV by the tether can be evaluated, as we perform in Part III with the study of the forces applied on the cable.

In both models, the umbilical is supposed to be neutrally buoyant with no variation of length, as in assumptions A1 and A2. More generally, it may be noted that the greatest interest of our model is the sliding element model, little studied in the literature where only fixed elements are generally considered. These sliding elements are at the center of the self-management strategy we propose to avoid entanglement and control the shape of the umbilical. This idea is closer to the work in [31] which simulates the dynamics of a variable-length cable in order to reduce its action on the ROV. In this study, fixed buoys are used to relieve some of the cable's weight. The control of the tether shape is more limited than with our method, but it considers a much longer cable and its dynamics are provided where our study requires a quasi-static equilibrium hypothesis.

10.5. Umbilical in presence of waves

In presence of waves, the position O of the boat becomes sinusoidal, impacting the position of the anchor A, and then buoys' positions and forces inside the umbilical. When the anchor does not touch the seafloor, this one can keep the umbilical stretched during the descent phase if its weight allows it to accelerate and fall faster than the wave, as described more in [37]. However, in case where the anchor touches the seafloor (permanently or temporally due to the waves' oscillations), the umbilical cannot be kept taut continuously, which can be dangerous for the material and lead to a cable breakage.

To avoid this problem, this section proposes a strategy to counter the wave's effect on the umbilical between the anchor and the ROV while avoiding an umbilical breakage, illustrated in Figure 11. Here, the umbilical between the boat

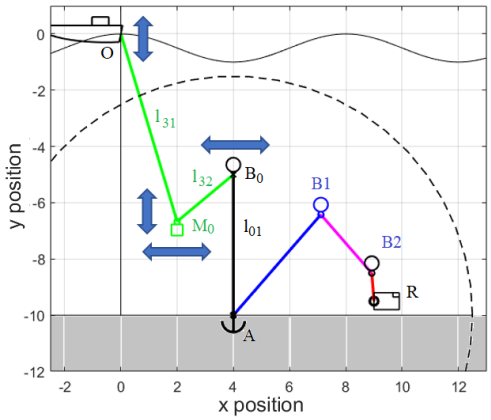

Figure 11: System to counter-balance wave effect on the umbilical and the ROV. Green: additional cable l_3, fixed buoy B_0 and sliding ballast M_0. The system in green allows to prevent waves' effects in the umbilical between A and R and avoid cable breakage.

O and the anchor A is divides in two parts. The first part l_3 between the boat and a fixed buoy B_0, the second l_{01} between the buoy B_0 and the anchor A. A sliding ballast $M0$ can move freely on the cable l_3 between O and A. The force of the ballast is chosen such it can accelerate and fall faster than the wave but stay smaller than the buoy's strength. Moreover, the anchor's weight is much stronger than the force of buoy B_0. The anchor A is put on the seafloor at y_{floor}. Since the influence of waves is maximum at the surface and decreases with depth, to become negligible, the length l_{01} is chosen such direct waves influence on the buoys B_0, B_1 and B_2 is negligible, *i.e.* one has at least $l_{01} < y_{\text{floor}} - h_w$ where h_w the wave's height. Finally, the length l_3 is chosen such the ballast can never touch the seafloor and cannot come in contact with the buoy $B0$, *i.e.* $l_3 < y_{\text{floor}} - \left(h_w + h_B\right)$ and $y_{\text{floor}} + h_w < l_3 + l_{01}$ where h_B the ballast height.

Using this system, when boat moves due to the action of the wave, the sliding ballast falls or works in opposition to keep the cable l_3 stretched in all situations, while the buoy B_0 oscillates to absorb the waves' effect, and the anchor stays immobile on the seafloor. Since the anchor stays immobile, no action from the waves affects the part of the umbilical between A and R.

11. Conclusion

This paper presents a novel approach to passively manage the umbilical of an ROV by adding additional elements such as ballasts, buoys, or an oriented thruster. The purpose is to stretch the umbilical in a controlled manner, ensuring a predictable shape and preventing entanglement with obstacles or itself. These elements can either be fixed or move freely along the umbilical, with stops in place to restrict constant contact. Unlike previous studies, this proposal introduces a general model capable of estimating the three-dimensional shape of the umbilical regardless of the applied force's orientation, allowing to consider the presence of underwater currents, passive or motorized elements on the tether, and the inclusion or exclusion of a TMS. The geometry and forces applied upon the umbilical are calculated using a quasi-static assumption.

The model provides a good vision of the system, allowing to build a umbilical equipment and observe its behavior. Example of different set up, adapted to specific missions, are proposed and tested in pool. The limits of the method have been discussed, specifically the computation time which can be improved. Suggestions for improvement have been made.

These improvements will be the subject of future works. Future works will also study the dynamics instead of a quasi-static equilibrium, with also variations of the sea current and uncertainties on parameters. Finally, measurements at sea during a true mission will be performed. the curvature of the cable will also be taken into account.

Acknowledgment

We acknowledge support from the Centre National de la Recherche Scientifique (CNRS) and Laboratoire des sciences et techniques de l'information, de la communication et de la connaissance (Lab-STICC). The author declares that there is no conflict of interest.

References

[1] BA Abel. Underwater vehicle tether management systems. In *Proceedings of OCEANS'94*, volume 2, pages II–495, 1994.

[2] O. Blintsov. Development of the mathematical modeling method for dynamics of the flexible tether as an element of the underwater complex. *Eastern-European Journal of Enterprise Technologies*, 1 (7):4–14, 2017.

[3] L. Brignone, E. Raugel, J. Opderbecke, V. Rigaud, R. Piasco, and S. Ragot. First sea trials of hrov the new hybrid vehicle developed by ifremer. In *Oceans 2015-genova*, pages 1–7, 2015.

[4] B. Buckham and M. Nahon. Dynamics simulation of low tension tethers. In *IEEE Conference Proceedings Oceans*, volume 2, pages 757–766, 1999.

[5] D. Bulić, D. Tolić, and I. Palunko. Beam-based tether dynamics and simulations using finite element model. *In Proc. IFAC-PapersOnLine*, 55(15):154–159, 2022.

[6] R. D. Christ and R. L. Wernli Sr. *The ROV manual: a user guide for observation class remotely operated vehicles*. Elsevier, 2011.

[7] T. Crandle, G. Cook, and E. Celkis. Tradeoffs between umbilical and battery power in rov performance. In *IEEE OCEANS 2017-Anchorage*, pages 1–6, 2017.

[8] J. Drupt, C. Dune, A. I. Comport, and V. Hugel. Validity of the catenary model for moving submarine cables with negative buoyancy. In *3rd workshop on RObotic MAnipulation of Deformable Objects: challenges in perception, planning and control for Soft Interaction (ROMADO-SI)*, 2022.

[9] J. Drupt, C. Dune, A. I Comport, S. Seillier, and V. Hugel. Inertial-measurement-based catenary shape estimation of underwater cables for tethered robots. In *In proc. IEEE/RSJ International Conference on Intelligent Robots and Systems (IROS)*, pages 6867–6872, 2022.

[10] R. G. Duncan, Mark E. Froggatt, S. .T Kreger, R. J. Seeley, D. K. Gifford, A. K. Sang, and M. S. Wolfe. High-accuracy fiber-optic shape sensing. In *Sensor Systems and Networks*, volume 6530, page 65301S, 2007.

[11] O. A. Eidsvik and I. Schjølberg. Time domain modeling of rov umbilical using beam equations. *IFAC*, 49(23):452–457, 2016.

[12] O. A. N. Eidsvik and I. Schjølberg. Finite element cable-model for remotely operated vehicles (rovs) by application of beam theory. *Ocean Engineering*, 163:322–336, 2018.

[13] M. Fabricius, D. Ø. Tarp, R. W. Kristensen, J. M. Andersen, J. Liniger, and S. Pedersen. Modelling and validation of a remotely operated towed vehicle and computational cost analysis of umbilical cable. *IFAC*, 56(3):415–420, 2023.

[14] Richard Phillips Feynman. The feynman lectures on physics. *(No Title)*, 1:46, 1963.

[15] M. Filliung, J. Drupt, C. Peraud, C. Dune, N. Boizot, A. Comport, C. Anthierens, and V. Hugel. An augmented catenary model for underwater tethered robots. In *In Proc. IEEE ICRA 2024*, 2024.

[16] J. E. Frank, R. Geiger, D. R. Kraige, and A. Murali. Smart tether system for underwater navigation and cable shape measurement, 2013. US Patent 8,437,979, URL https://patents.google.com/patent/US8437979B2/en.

[17] O. Ganoni, R. Mukundan, and R. Green. A generalized simulation framework for tethered remotely operated vehicles in realistic underwater environments. *Drones*, 3(1):1, 2018.

[18] O. Ganoni, R. Mukundan, and R. Green. Visually realistic graphical simulation of underwater cable. *Computer Science Research Notes*, 2018.

[19] F. González, A. de la Prada, A. Luaces, and M. González. Real-time simulation of cable pay-out and reel-in with towed fishing gears. *Ocean Engineering*, 131:295–307, 2017.

[20] Sung Min Hong, Kyoung Nam Ha, and Joon-Young Kim. Dynamics modeling and motion simulation of usv/uuv with linked underwater cable. *Journal of Marine Science and Engineering*, 8(5):318, 2020.

[21] M. Incera, L. Valbuena, J. Falcón, E.L. González, M. González-Porto, L. Martín-García, P. Martín-Sosa, and J. Gago. Assessment of seabed litter at concepción seamount (canary island) using a remotely operated towed vehicle. *Environmental Pollution*, page 123654, 2024.

[22] N. Kapetanović, K. Krčmar, N. Mišković, and Đ. Nađ. Tether management system for autonomous inspection missions in mariculture using an asv and an rov. *In Proc. IFAC-PapersOnLine*, 55(31):327–332, 2022.

[23] O. Khatib, X. Yeh, G. Brantner, B. Soe, B. Kim, S. Ganguly, H. Stuart, S. Wang, M. Cutkosky, A. Edsinger, et al. Ocean one: A robotic avatar for oceanic discovery. *IEEE Robotics & Automation Magazine*, 23(4):20–29, 2016.

[24] M. Laranjeira, C. Dune, and V. Hugel. Catenary-based visual servoing for tethered robots. In *IEEE International Conference on Robotics and Automation*, pages 732–738, 2017.

[25] M. Laranjeira, C. Dune, and V. Hugel. Embedded visual detection and shape identification of underwater umbilical for vehicle positioning. In *OCEANS 2019-Marseille*, pages 1–9, 2019.

[26] M. Laranjeira, C. Dune, and V. Hugel. Catenary-based visual servoing for tether shape control between underwater vehicles. *Ocean Engineering*, 200:107018, 2020.

[27] A. Lasbouygues, S. Louis, B. Ropars, L. Rossi, H. Jourde, H. Délas, P. Balordi, R. Bouchard, M. Dighouth, M. Dugrenot, et al. Robotic mapping of a karst aquifer. In *IFAC: International Federation of Automatic Control*, 2017.

[28] M. B. Lubis, M. Kimiaei, and M. Efthymiou. Alternative configurations to optimize tension in the umbilical of a work class rov performing ultra-deep-water operation. *Ocean Engineering*, 225:108786, 2021.

[29] L. Mathieu. *Using a towed undulating platform to measure ocean velocities and to estimate turbulent dissipation rate*. PhD thesis, EPFL, 2019.

[30] S. Pedersen, J. Liniger, F. F. Sørensen, and M. von Benzon. On marine growth removal on offshore structures. In *OCEANS 2022*, pages 1–6, 2022.

[31] S. Prabhakar and B. Buckham. Dynamics modeling and control of a variable length remotely operated vehicle tether. In *Proceedings of OCEANS 2005 MTS/IEEE*, pages 1255–1262 Vol. 2, 2005.

[32] A. G. Rumson. The application of fully unmanned robotic systems for inspection of subsea pipelines. *Ocean Engineering*, 235:109214, 2021.

[33] H. Stuart, S. Wang, O. Khatib, and M. R. Cutkosky. The ocean one hands: An adaptive design for robust marine manipulation. *The International Journal of Robotics Research*, 36(2):150–166, 2017.

[34] M. Such, J. R. Jimenez-Octavio, A. Carnicero, and O. Lopez-Garcia. An approach based on the catenary equation to deal with static analysis of three dimensional cable structures. *Engineering structures*, 31(9):2162–2170, 2009.

[35] O. Tortorici, C. Anthierens, V. Hugel, and H. Barthelemy. Towards active self-management of umbilical linking rov and usv for safer submarine missions. *IFAC-PapersOnLine*, 52(21):265–270, 2019.

[36] C. Viel. Self-management of rov umbilical using sliding buoys and stop. *IEEE Robotics and Automation Letters*, 7(3):8061–8068, 2022.

[37] C. Viel. Self-management of the umbilical of a rov for underwater exploration. *Ocean Engineering*, 248:110695, 2022.

[38] C. Viel, J. Drupt, C. Dune, and V. Hugel. Rov localization based on umbilical angle measurement. *Ocean Engineering*, 269:113570, 2023.

[39] Christophe Viel. Self-Management of ROV Umbilical using sliding element: a general 3D-model - Full version. working paper or preprint. https://hal.science/hal-04157011, July 2023.

[40] M. Vigo, J. Navarro, J. Aguzzi, N. Bahamón, J. A. García, G. Rotllant, L. Recasens, and J. B. Company. Rov-based monitoring of passive ecological recovery in a deep-sea no-take fishery reserve. *Science of the Total Environment*, 883:163339, 2023.

[41] M. von Benzon, F. F. Sørensen, E. Uth, J. Jouffroy, J. Liniger, and S. Pedersen. An open-source benchmark simulator: Control of a bluerov2 underwater robot. *Journal of Marine Science and Engineering*, 10(12):1898, 2022.

[42] C. Zhao, P. R. Thies, and L. Johanning. Offshore inspection mission modelling for an asv/rov system. *Ocean Engineering*, 259:111899, 2022.